Building and Environment 264 (2024) 111892

Contents lists available at ScienceDirect

Building and Environment

journal homepage: www.elsevier.com/locate/buildenv

On the suitability of dispersion models of varying degree of complexity for air quality assessment and urban planning

William R. Patiño [a,*], Ondřej Vlček [a], Petra Bauerová [a], Michal Belda [c], Martin Bureš [b,d], Kryštof Eben [b], Vladimír Fuka [c], Jan Geletič [b], Radek Jareš [d], Jan Karel [d], Josef Keder [a], Pavel Krč [b], Jelena Radović [c,d], Hynek Řezníček [b], Adriana Šindelářová [a], Jaroslav Resler [b]

[a] Czech Hydrometeorological Institute, Na Šabatce 2050/17, 143 00 Prague 12, Czech Republic
[b] Institute of Computer Science, Czech Academy of Sciences, Pod Vodárenskou věží271/2, 182 00 Prague 8, Czech Republic
[c] Department of Atmospheric Physics, Charles University Prague, V Holešovičkách 2, 180 00 Prague 8, Czech Republic
[d] ATEM – Studio of ecological models, Roztylská 1860/1, 148 00 Prague 4, Czech Republic

ARTICLE INFO

Keywords:
Dispersion modeling
Particulate matter
Air pollution
Urban climate
Microscale

ABSTRACT

The development of integrated urban services requires the implementation of informative tools that provide a balance between quality, time and costs for air quality assessment. Within this framework, three modeling techniques with different levels of complexity were compared during a winter inversion episode against PM_{10} concentrations measured in a built-up area in Prague (Czech Republic) characterized by heavy traffic. Although the Gaussian model ATEM satisfied the common statistical-performance criteria, the predictions poorly represented the spatial variability of concentrations in the study domain. The Lagrangian model GRAL provided a better simulation of the effects of terrain and vortice formation inside street canyons, but tended to overpredict the influence of these phenomena. Finally, the most sophisticated of the three models, the Large-Eddy Simulation model PALM, demonstrated the best performance based on an exhaustive analysis of the model outputs in the temporal and spatial dimensions. After model comparison, a sensitivity test of the selected models to the driving meteorology and emissions inputs was carried out. While advanced models can simulate complex urban environments, their suitability for use in urban planning is subject to further considerations, such as computational cost, user expertise, and the usefulness of the output. Thanks to increasing computation power and intensive work on the entire modeling chain, sophisticated models could become routine tools for use in regulatory applications, contributing to future integrated urban service provision.

1. Introduction

Urban areas are shaped by a complex interplay of geographical, morphological, climatic, ecological, and anthropogenic factors. The unique features of each city pose challenges for developing decision-support systems that effectively simulate urban environments. From this perspective, street canyons are of special concern, given the increased likelihood of the exposure of pedestrians, cyclists, drivers, and residents to pollutant concentrations that might exceed current air-quality standards [1]. Pollution dispersion in street canyons is significantly constrained by the physical barriers formed by the building walls and by the unique microclimatic conditions along the street, which create 'hotspots' where recirculation flows trap air pollutants [2,3]. Consequently, the mean exposure time, or the time a pollutant remains in a respirable region, can be considerably longer in street canyons than in open areas [4].

Cities and local municipalities are usually not equipped to deal with local- or microscale issues in such fine detail, and the legislation, supplementary tools, data, or model-based information required to address such issues are often missing or outdated. As a result, air-quality limits in urban areas can be exceeded, especially during periods of strong atmospheric inversion. Since the Great London Smog in 1952 [5], particulate matter (PM) has been considered a major factor in the context of the health hazards caused by urban pollution, especially in Central and Eastern Europe, Northern Italy, and the Balkans [6]. PM is associated with increased daily mortality due to cardiovascular diseases such as stroke, ischemic heart disease, or myocardial infarction, as well as respiratory conditions, including chronic obstructive pulmonary disease, asthma, and bronchitis [7].

Air quality or meteorological forecast modeling of the stable conditions during persistent wintertime thermal inversions is challenging [8–

* Corresponding author.
E-mail address: william.patino@chmi.cz (W.R. Patiño).

https://doi.org/10.1016/j.buildenv.2024.111892
Received 30 April 2024; Received in revised form 4 July 2024; Accepted 25 July 2024
Available online 2 August 2024

10], and few studies have addressed the simulation and accurate prediction of dispersion during such situations. The performance of dispersion models has been tested for urban settings and street canyons [11,12], but scarcely any [3,13–15] have focused on winter conditions.

Owing to the uniqueness of the urban environment and the interconnectedness of its components, assessing some parameters from a single perspective may result in adverse impacts in different parts of the system being overlooked; for instance, improvements in thermal comfort may negatively affect air quality (more examples can be found in a detailed sensitivity study for Prague; [16]). Therefore, efforts are underway to develop universal tools for multi-level microscale analysis of meteorological variables. One of these tools, the Large-Eddy Simulation (LES) model PALM [17], explicitly resolves turbulence within the urban boundary layer, and can thus accurately capture atmospheric processes within densely built and complex urban areas [18]. Despite the advantages of microscale models that apply the LES core, some drawbacks (e.g., high computational costs, the need for high-resolution input data, and user expertise) limit their practical application. Several other types of models with varying degrees of complexity are conventionally used for forecasting and decision-making. On the one hand, Gaussian plume models are based on the assumption of normal distribution for the horizontal and vertical crosswind dispersion of pollutants in the plume. They portray the pollutants emitted continuously as a single plume that expands in two dimensions over time. Gaussian models assume steady-state conditions, in which both emissions and meteorology remain constant over time. They account for terrain only in a very simplified way, and have limited capacity for modeling low wind speeds, chemical transformations, or the effects of complex building structures. Their results, supported by empirical observations, have served as regulatory tools in many countries for nearly five decades, and are often still used [19]. For example, the ATEM (Ateliér Ekologických Modelů) and SYMOS (Systém modelování stacionárních zdrojů) Gaussian models have been used for regulatory purposes in the Czech Republic [20], and the ATEM model, in combination with a regional chemical transport model, is used for annual air quality assessment in Prague. On the other hand, the more sophisticated Lagrangian models (e.g., GRAL; [21]) simulate the motion of the air masses, represented by marked particles, that transport pollutants emitted at regular intervals from the source. The transport of each particle is simulated based on the mean wind and diffusion, related to the turbulent wind velocity fluctuations [22]. Although these models achieve better accuracy for complex terrain and non-stationary emissions than the Gaussian models, they require a better description of topography and wind fields. Consequently, utilizing both Gaussian and Lagrangian models provides a promising solution for achieving fast and effective modeling with reasonable results at the expense of reduced complexity in describing the phenomenon. Such models have been widely used and validated (see, e.g., [14,23–25]).

Multiple reviews on the techniques and models frequently used for air-pollution and dispersion assessment have been published (e.g., [26–32]). An extensive comparison of models, including Gaussian, Lagrangian, and computational fluid dynamics (CFD) models, is presented in [11,33]. However, for the practical application of modeling studies, the scientific evaluation of modeling tools is only one of many parameters to consider. Stakeholders (including governments, city councils, and local municipalities) must often prioritize their own criteria and information flow within urban modeling frameworks, and collaborative efforts between the scientific community and decision-makers are essential for refining model setups and configurations to satisfy specific urban needs. Moreover, an effective communication of modeling results via spatially explicit storytelling approaches can enhance their usability in decision-making processes.

Consequently, this study aims to: (1) evaluate modeling predictions against air quality measurements; (2) compare the information on spatial variability generated by three different dispersion models; (3) identify possible sources of error; (4) discuss strengths and weaknesses, and explore the potential of model application for integrated urban service provision [34].

2. Study area and methods

2.1. Study area

The study area, also called 'domain', is located in Prague, the capital of the Czech Republic. With a population exceeding 1.35 million in the city and more than 1.4 million in the metropolitan area, Prague could be considered a European agglomeration. The city exhibits unique conditions related to both its historical development and current expansion. Transport infrastructure, planned and developed mostly between the 1940s and 1970s, is overloaded by cars, especially during morning and afternoon traffic peaks, placing an additional burden on air quality. The analyzed domain covers an area of 1200 m × 1600 m (Fig. 1), centered on Legerova and Sokolská streets, north–south oriented one-way boulevards, which currently create the main arterial road through the city. The district was designed and built between the 1880s and 1890s. Up to the 1970s, both streets represented typical boulevards in compact mid-rise build-up. The relevance of transportation and traffic increased with the building of the Nusle bridge, which brought transit directly to the city center and, consequently, to the northern parts of Prague. Currently, the daily mean traffic intensity exceeds 35 thousand cars in each direction. Both street canyons could be classified as nearly symmetric, approximately 18 m wide, with an aspect ratio (ratio of canyon height to canyon width) between 1.0 and 1.3. The adjacent blocks of buildings favor poor air circulation, strengthening the stagnation of air pollutants. Both streets are practically without urban greenery; trees are located only inside closed courtyards.

2.2. Meteorological conditions and measurements

Episodes with elevated PM concentrations occur with greater intensity during inversion situations, which are typical in winter. This study focuses on the inversion between 13 and 15 February 2023. The period was marked by the presence of a stationary high-pressure system across western and central Europe. Compared to other periods in the 2022/2023 winter season, this episode exhibited an especially strong temperature inversion (Fig. 2) due to warm advection in the higher levels, which moved to lower altitudes. The inversion weather was accompanied by predominantly low wind speeds (Figs. A.1–A.2) and broken-to-overcast cloudiness. Such conditions in February are not favorable for air-pollution dispersion in central Europe [36]; therefore, this situation resulted in high PM_{10} concentrations (Fig. 3).

Within the TURBAN project (https://project-turban.eu), a targeted measurement campaign was carried out from 30 May 2022 to 28 March 2023 to collect observations relevant for model validation. The meteorological observations were collected using a mobile meteorological mast (MM), a microwave radiometer (MWR), and a Doppler LIDAR. Pollutant concentration in the area was measured using a network of 20 low-cost air quality sensor (LCS) units, out of which 14 were operational during the study period. The measurement campaign data were supplemented by data from permanent stations operated by the Czech Hydrometeorological Institute (CHMI): a meteorological station located at roof level, roughly 30 m above ground, in Karlov (P1PKAR01, WMO ID 11519) and the traffic air quality monitoring station Legerova (ALEGA) (see Fig. 1 and Table 1 for observation and sensor locations). Most of the LCSs were located in streets with the highest traffic-pollution load: three were placed along Sokolská Street (S10, S11, and S12), two in Rumunská Street (S13 and S20) , and four along Legerova Street (S2, S5, S14, and S15). Others were installed in 'background areas', such as the PVK garden (S19) and a school courtyard (S7 and S9). The remaining two LCSs were located at considerable distances from the pollution hotspots and at greater heights: in Karlov (S3) and at the Hotel Le Palais (S16). Some sensors were placed in pairs at different heights on the facades of buildings. The data retrieved was corrected based on sensor co-measurements, using reference air quality data from the monitoring station Libuš (ALIBA) at the beginning and the end of the campaign. A detailed description of the equipment implemented, collected data, and correction methods applied is available in [35].

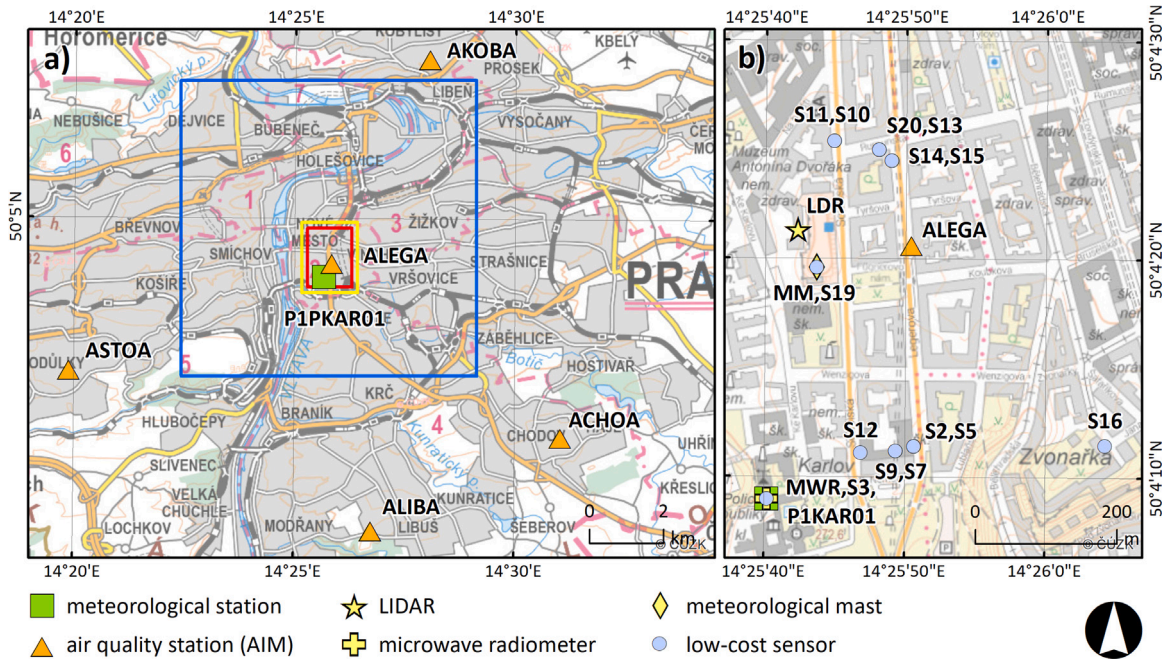

Fig. 1. (a) Extent of the common modeling domain (red), PALM parent domain (blue), and GRAMM domain (yellow), and the location of air quality and meteorological stations used in this study. (b) Close-up view with measurement locations for the study period (further details are available in [35]). (For interpretation of the references to color in this figure legend, the reader is referred to the web version of this article.)

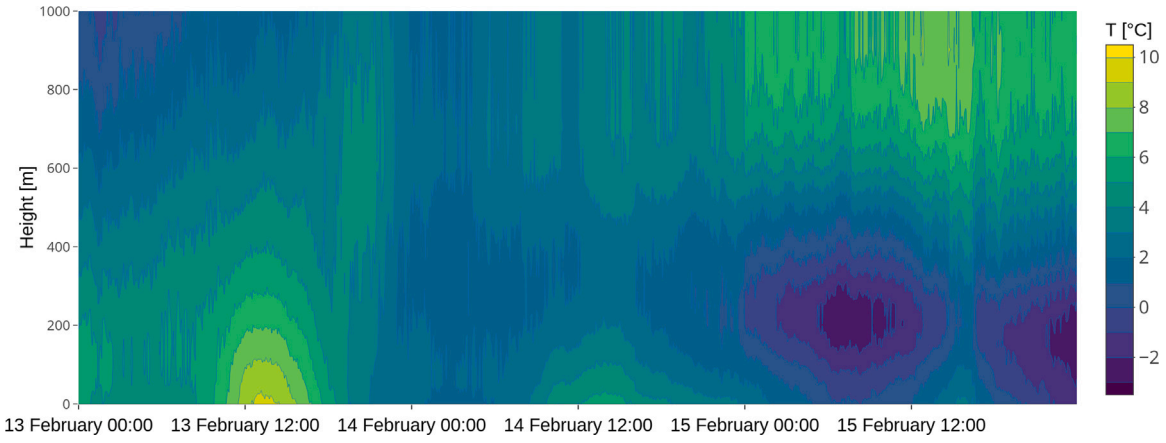

Fig. 2. Temperature profile measured by a microwave radiometer (MWR) located at the Karlov station (P1PKAR01).

Table 1
Receptor location and measuring height. Further specifications are found in [35].

Group	Receptor	Y UTM33N [m]	X UTM33N [m]	Position	Height [m AGL]
Background	S19	5 546 805	459 125	–	2.6
	S9	5 546 549	459 237	Low	6.9
	S7			High	4.7
Roof	S3	5 546 499	459 047	–	31.1
	S16	5 546 549	459 529	–	22.5
Traffic	ALEGA	5 546 834	459 259	–	3
	S12	5 546 541	459 183	–	5.9
	S11	5 546 983	459 149	Low	5.5
	S10			High	12.2
	S20	5 546 971	459 214	Low	4.6
	S13			High	14.8
	S14	5 546 955	459 233	Low	9.2
	S15			High	14.6
	S2	5 546 551	459 265	Low	5.8
	S5			High	13.2

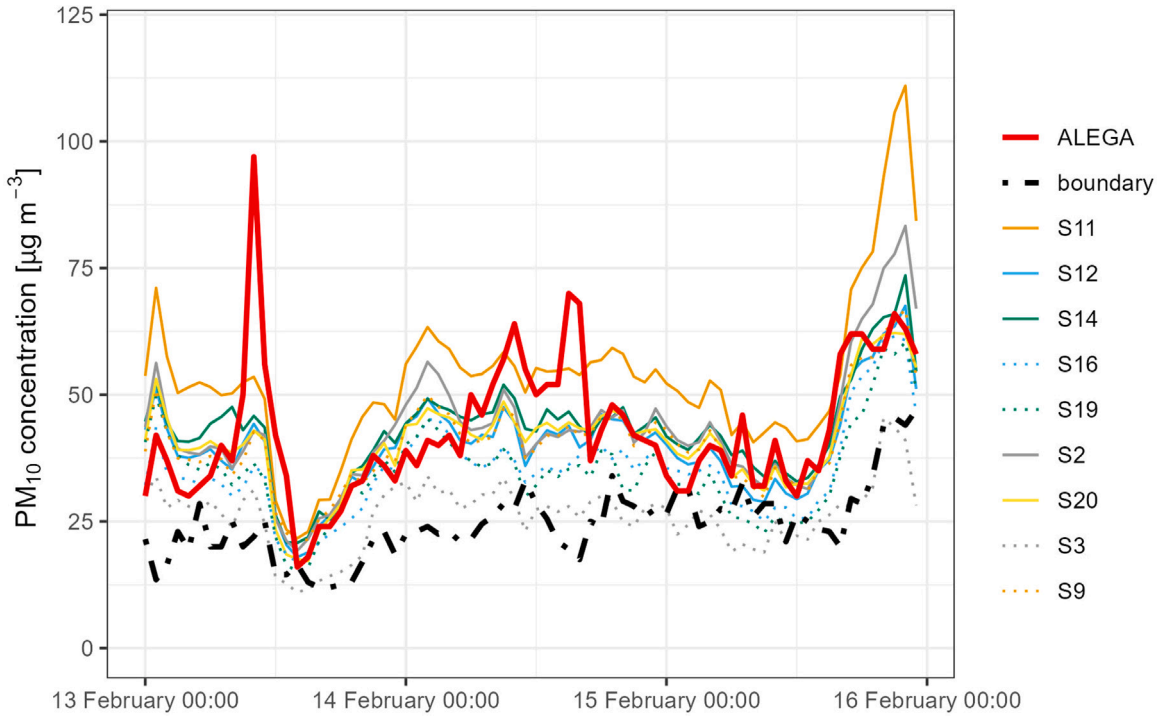

Fig. 3. PM_{10} concentration (hourly average) measured in the study domain. ALEGA: permanent traffic air quality monitoring station Legerova, boundary: boundary concentrations used by the models, Sx: sensors (solid lines – sensors in street canyon, dotted lines – sensors at a distant location from the roads or background location). For better readability, only the results from the lower sensor are displayed at locations where pairs of sensors were installed.

2.3. Description of the models

Each model differs in its principles, algorithms, and inputs needed. Moreover, each model requires different levels of detail of meteorological and topographical data. The following subsections contain a summary of the three models used.

2.3.1. ATEM

ATEM (v. 1.0.1.0) [37] is a Gaussian dispersion model developed to calculate concentrations of passive pollutants from point, line, and area sources. ATEM is an older-generation model; i.e., it relies on stability classes, rather than on the Monin–Obukhov similarity theory, for the determination of dispersion parameters. Atmospheric stability is determined from the vertical temperature-gradient and follows the classification proposed for the Czech Republic by Bubník & Koldovský (BK; [38,39]).

Topography is considered by incorporating the heights of reference points and emission sources, obtained from a 1 m resolution digital terrain model of Prague. Therefore, the model incorporates a three-dimensional (3D) relationship between source and point. However, the ATEM model is unable to perform orographic correction, i.e., it does not divert flow around obstacles. The spread of pollution is parameterized entirely by Gaussian scattering on the source-point connection. Moreover, the model allows only for the calculation of the whole year time series. Owing to the resulting number of grid cells and the computational demand, a square grid of computational points with 24 m spacing was implemented. Along the major roads in the domain, a 20 m buffer zone was used, with spacing of 6 m.

The ATEM meteorological input comprises an annual time series of wind speed, wind direction, and temperature gradient, obtained from measurements at Karlov station and MWR profiles. The temperature gradient ($-\mathrm{d}T/\mathrm{d}z$) reflects the temperature difference between 2 m and 100 m AGL. Based on the BK scheme, the resulting classification of the study-period data revealed primarily convective conditions (61%), with the remainder ranging from slightly stable to neutral. The reason for this particular classification is that the range of convective conditions in the BK scheme was established based on a temperature gradient >0.8 °C/100 m; in contrast, the Pasquill–Gifford (PG) stability class scheme determines convective conditions for values >1.5 °C/100 m [40]. Consequently, the correspondent dispersion parameters and plume-rise coefficients differ substantially from those generated by the other Gaussian models, as has been previously documented [41].

2.3.2. GRAL

GRAL (v. 22.03) [21] is a Lagrangian particle model developed to simulate the dispersion of chemically non-reactive pollutants in complex terrain and built-up areas. The system is coupled with GRAMM, a non-hydrostatic mesoscale model, which calculates quasi-steady-state solutions for the flow field, based on meteorological situations categorized according to the PG stability classes. A prognostic microscale module [42], based on Reynolds-averaged Navier–Stokes equations and the widely used standard $k-\epsilon$ turbulence model, is integrated into GRAL to handle the effects of obstacles.

Dispersion simulations were computed in transient mode, where the last position of released particles is stored as soon as the dispersion time expires. In this way, the stored transient particles are released and tracked together with newly emitted particles in the subsequent weather situation. The concentrations are then calculated using the box-counting method. The computational particles released from line sources were initially equally distributed from the ground level up to a height of 3 m, in order to consider traffic-induced turbulence [43].

The GRAMM model was implemented in a domain of 1500 m × 1900 m (Fig. 1), with a horizontal resolution of 50 m and a vertical resolution of 10 m (with vertical stretching), with a height of 1500 m. Terrain elevation (at 1 m resolution) was obtained from a raster layer of Prague. The land-cover classification developed for PALM using the WRF model [44], complemented with the Corine Land Cover 2018 database, was employed to determine the land-use characteristics (including surface roughness length, albedo, and soil moisture) for calculating the surface energy balance. The internal-flow field grid and concentration grid were computed using a horizontal and

vertical resolution of 2 m (with vertical stretching) and a maximum height of ca. 700 m.

The GRAL meteorological input requires a time series of wind speed, wind direction, and a stability parameter. The temperature gradient (calculated from the same levels used for the ATEM model) was used to establish the PG classes, following the scheme proposed by the National Oceanic and Atmospheric Administration NOAA [45]. Analysis of the meteorological measurements revealed predominantly neutral (58%) and stable (33%) conditions during the study period.

2.3.3. PALM

PALM (v. 23.04) [17] is a state-of-the-art model designed to capture the flow field, energy transfer, and chemistry within the urban canopy with the highest spatial and temporal resolution possible. PALM system incorporates the LES core to solve the non-hydrostatic, filtered, Boussinesq-approximated, incompressible Navier–Stokes equations (with 1.5 order turbulence closure), along with various modules for investigating the urban boundary layer, including a land-surface model (LSM; [46]), building-surface model (BSM; [47]), radiative-transfer and plant-canopy models (RTM and PCM; [48]), with online nesting (NEST; [49]) and mesoscale nesting (MESO; [50]). Although it also includes a chemical-transport model [51], this was not implemented here.

The meteorological data required to run PALM include the detailed structure of all wind components, potential temperature, air moisture and pressure, and incoming short-wave and long-wave radiation. Therefore, PALM is typically driven by a mesoscale Numerical Weather Prediction model (NWP) run that provides all necessary initial and boundary conditions (IBC). For this study, the ALADIN model [52] was selected in the configuration used for operational weather-prediction in the Czech Republic.

PALM was configured in two nested domains (see Fig. 1) to simulate all mixing-layer processes properly. The outer 'parent' domain has an extent of 8000 m × 8000 m, with a horizontal and vertical resolution of 10 m (with vertical stretching) and a height of 2750 m. The nested 'child' domain corresponds with the modeling domain, with a horizontal and vertical resolution of 2 m (without stretching) and a height of 320 m. The modeling setup requires complete information about land cover, including the surface materials of the ground and walls (with their heat capacities and albedos) and the position and type of trees in the domain. In this study, PALM was configured with full 3D geometry, allowing the modeling of objects such as bridges and multilevel crossroads. A detailed description of the domains and setting of the model can be found in [10].

2.4. Emissions

Emissions from mobile sources (road traffic, railways, and river shipping) and residential heating were included. In the study area, traffic was responsible for 90.7% of PM_{10} emissions.

Emissions from transport sources were obtained using the transportation emission model of MEFA et al. [53], a regulatory model designated by the Ministry of Environment of the Czech Republic. The model considers factors such as meteorological conditions, type of road surface, traffic-flow speed and composition, road gradient, number of vehicles on the road, and the emission characteristics of the individual car types. The emission calculation is based on data from the traffic census and regular surveys of the composition of the transportation fleet in Prague [54]. Census data (provided by the Prague Technical Administration of Roads) was utilized for all streets for which it was available, although for Legerova and Sokolská streets, hourly traffic-intensity data were used. For smaller streets not covered by regular traffic surveys, the spatial and temporal distribution of traffic intensity was based on analysis and evaluation of relevant urban-planning studies for the particular area and on information such as street type, location, traffic regime, and pavement type. Dust resuspension was computed for the main roads according to the methodology published by the Ministry of the Environment [55], based on US Environmental Protection Agency (EPA) methodology AP-42 [56], and was fitted for the conditions of the Czech Republic. The time profiles used for emissions from roads are shown in Fig. A.3.

For garages and parking lots, the results of the TH03030496 project [57] were used, and for bus stations, publicly available data about transportation were gathered from the Prague Public Transit Company. For emissions from rail transport (diesel locomotives), emission factors from the EMEP/EEA Air Pollutant Emission Inventory Guidebook 2019 [58] were applied to train-ride data obtained from the Railway Administration. Emissions from river shipping were obtained from the Czech Hydrometeorological Institute (CHMI) national database and were distributed spatially to account for the area of the river.

Emissions from residential heating were determined using calculations based on data provided by the CHMI and the Czech Statistical Office. First, the national emission totals were distributed over a 0.01° × 0.01° grid according to the surfaces of the locally heated buildings, separately for each of the primary fuel types. Second, total residential heating emissions within this grid were distributed to houses according to the number of floors. Finally, in the case of the ATEM and GRAL models, emissions were assigned to the corresponding building centroid with an effective height calculated as the number of floors times 3 m plus 12 m (a rough estimate to account for the roof/chimney and plume rise). In the case of the PALM model, residential heating emissions were placed at the rooftop with no plume-rise taken into account. For time disaggregation, profiles of daily supplies of natural gas were used (category 'DOM4' using gas for heating only; [59]) and were complemented using daily SNAP 2 profiles [60]. The emission sources were processed into hourly emission flows in the PALM input data standard using the FUME emissions model, recently extended for this purpose [61].

Spatial transformation of the line- and point-emission sources to the corresponding areas for PALM input was done using surrogates (i.e., the area of roads and parking places as a surrogate for traffic emissions, and that of building roofs as a surrogate for local heating source emissions). This both ensures the reasonable spatial distribution of emissions in the street canyon and reduces the gradients of the emission field, making the model less prone to numerical inaccuracy [62].

2.5. Initial and boundary conditions for air pollutants

The initial and boundary conditions for air pollutants (PM_{10}) were calculated as the median values of measurements from background air quality stations in the surroundings of the PALM parent domain (Fig. 1). Since neither ATEM nor GRAL allows for direct inclusion of these data in calculations, the 'boundary' concentrations were added to the time-series calculated for each measurement location, and to the gridded outputs during results post-processing. However, GRAL does not enable easy mass export of gridded results for each hour, so the 'boundary' concentrations could not be taken into account for the calculation of percentile maps.

The observations were complemented by the CAMS model-based vertical profiles [63] scaled to the observed near-surface value for PALM input. Hence, the boundary PM10 concentrations included secondary aerosols as well. Nonetheless, given the difference in the timescale of secondary aerosol formation (in the range of hours or days) and the typical period in which the air masses pass through the PALM domain (in minutes or tens of minutes), generation of secondary aerosols inside the modeling domain was not considered.

2.6. Descriptive statistics used for model evaluation

The terms $\sigma^o = \sqrt{\sum_{i=1}^{n}(C_i^o - \overline{C^o})^2}$, $\sigma^m = \sqrt{\sum_{i=1}^{n}(C_i^m - \overline{C^m})^2}$ are the standard deviations of observed and modeled concentrations,

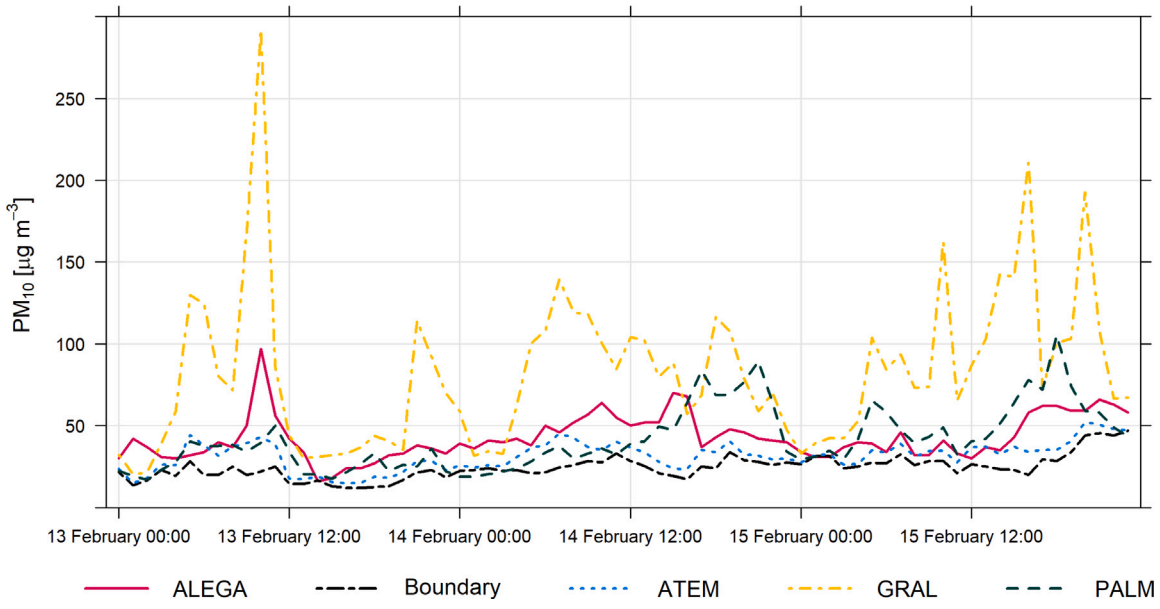

Fig. 4. Time series of PM_{10} concentrations computed using ATEM, GRAL, and PALM compared against the ALEGA monitoring-station measurement.

respectively. In addition to using standard measures such as the root-mean-squared error (RMSE) and sample correlation coefficient (r), supporting statistics such as the fraction of modeled values within a factor of 2 of the observed values (FAC2), fractional bias (FB), and the normalized mean square error (NMSE) were also calculated to evaluate model performance. The centered (de-biased) root-mean-square error (CRMSE), which is plotted in the Taylor diagram, was also considered. The FB and NMSE correspond to those used by Chang and Hanna [64].

$$\text{FAC2} = \text{Proportion of pairs } (C^o, C^m) \text{ such that } \frac{1}{2} \le C^m/C^o \le 2 \quad (1)$$

$$r = \frac{\frac{1}{n}\sum_{i=1}^{n}(C_i^o - \overline{C^o})(C_i^m - \overline{C^m})}{\sigma^o \sigma^m} \quad (2)$$

$$\text{FB} = \frac{\overline{C^o} - \overline{C^m}}{0.5(\overline{C^o} + \overline{C^m})} \quad (3)$$

$$\text{NMSE} = \frac{\overline{(C^o - C^m)^2}}{\overline{C^o}\ \overline{C^m}} \quad (4)$$

$$\text{RMSE} = \left[\frac{1}{n}\sum_{i=1}^{n}(C_i^o - C_i^m)^2\right]^{1/2} \quad (5)$$

$$\text{CRMSE} = \left[\frac{1}{n}\sum_{i=1}^{n}\left[(C_i^o - \overline{C^o}) - (C_i^m - \overline{C^m})\right]^2\right]^{1/2} \quad (6)$$

3. Results

3.1. Model evaluation

Model simulation results were compared against measurements taken at the ALEGA monitoring-station and at the locations of the LCS. For ATEM, the corresponding reference points were given the exact coordinates and height above ground of the measurement point. For GRAL and PALM, the modeled concentrations were retrieved from the grid cell in which the measurement was located, or from the nearest valid (i.e., non-building) grid cell. An exceptionally high value was recorded at the ALEGA monitoring-station on 13 February (Monday) at 10:00 UTC (at the beginning of the 1 h interval). Although this peak coincides with the peak in traffic emissions (Fig. A.3), it was not recorded at any other measurement location (Fig. 3). Since the variation in emissions over time for Legerova street differs substantially from those for the other roads, and since there were no other measurements on the west side of Legerova street, we could not state with certainty that this issue was caused by some strong temporary emission source not included in the models.

First, simulated concentrations were compared against the ALEGA monitoring-station time series. The ATEM model predictions mostly followed the boundary concentration curve and therefore underestimated the measured PM_{10} concentrations, especially for the daytime (Fig. 4). The only exception occurred on February 13, although the concentration was still underestimated by roughly half in the preceding hours. On the other hand, GRAL systematically overpredicted the measurements. For rush hours, in particular, the modeled concentrations were almost 2–3 times larger than the observed values, sometimes reaching unrealistic values. The predictions using PALM followed the daily trends in the measurements, with slightly underestimated concentrations during the morning of 14 February and an overestimation during the evening of the same day.

For the subsequent analysis, the stations were grouped by location type into traffic (stations located directly in the street canyon), background (stations further away from roads or in a closed courtyard) and roofs (stations located on the roofs of the buildings). As a reference, the statistics were also calculated for the boundary concentrations. An overview of model performance is provided by the Taylor Diagram (Fig. 5), which combines the correlation, standard deviation, and CRMSE: the correlation with observations was 0.4–0.6, CRMSE was ca. 10 µg m^{-3}, and the predictions exhibited lower standard deviations than the observations (i.e., less variability). There are, however, two remarkable exceptions: First, the correlation between the PALM predictions and traffic station observations was much worse than the other correlations, at ca. 0.2; the PALM predictions exhibited greater variability at traffic locations than the measured values; and the CRMSE was almost 18 µg m^{-3}. Second, the GRAL model exhibited similarly poor correlations between predictions and measurements at traffic stations as the PALM model, and the standard deviation of its predictions was more than three times larger than that of the observations; consequently, the CRMSE reached almost 40 µg m^{-3}. For the background stations, the standard deviation of the GRAL predictions was 1.5 times larger than that for observations, with a correlation of ca. 0.2 and CRMSE of ca. 15 µg m^{-3}.

Analyzing the statistics presented in Table 2 provides greater insight. Model performance was assessed against the acceptance criteria summarized by Hanna and Chang [65] for urban applications: FAC2

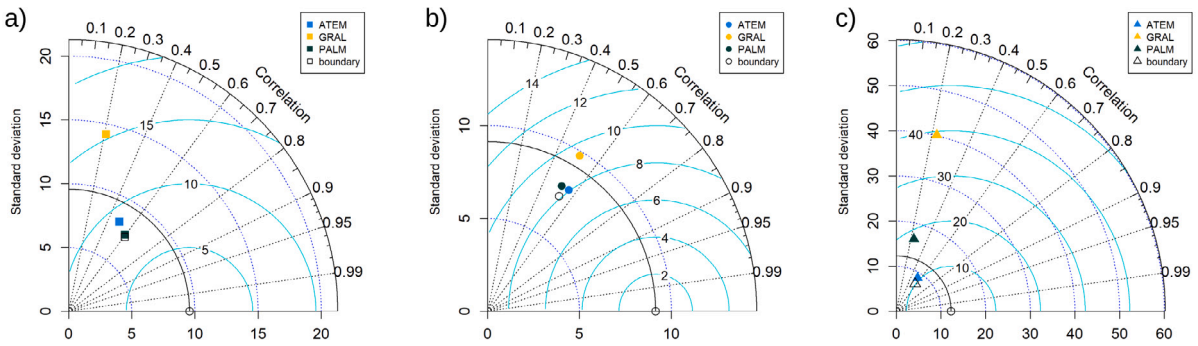

Fig. 5. Taylor diagrams based on PM_{10} hourly mean concentrations split by model for background (a), roof (b) and traffic stations (c).

Table 2
Performance metrics based on PM_{10} hourly mean concentrations. Values in bold are within the range recommended by Hanna and Chang [65]. The best statistics obtained for each group are highlighted in green.

Group[a]	Model	n	Mean obs [μg m^{-3}]	Mean mod [μg m^{-3}]	FAC2 [–]	r [–]	FB [–]	NMSE [μg m^{-3}]	RMSE [μg m^{-3}]
Background	ATEM	216	38.31	29.19	**0.95**	**0.50**	**0.27**	**0.15**	12.78
	GRAL			30.82	**0.87**	0.21	**0.22**	**0.25**	17.10
	PALM			25.57	**0.86**	**0.60**	**0.40**	**0.23**	14.98
	Boundary			24.51	**0.85**	**0.61**	**0.44**	**0.27**	15.83
Roof	ATEM	144	30.72	27.85	**0.99**	**0.56**	**0.10**	**0.09**	8.56
	GRAL			27.37	**0.98**	**0.51**	**0.12**	**0.12**	9.93
	PALM			26.12	**0.94**	**0.51**	**0.16**	**0.12**	9.64
	Boundary			24.51	**0.97**	**0.53**	**0.22**	**0.14**	10.22
Traffic	ATEM	720	44.64	30.83	**0.89**	**0.56**	**0.37**	**0.22**	17.23
	GRAL			62.20	**0.76**	0.23	**-0.33**	**0.67**	43.38
	PALM			41.78	**0.88**	0.24	**0.07**	**0.18**	18.28
	Boundary			24.51	**0.63**	**0.60**	**0.58**	**0.46**	22.38

[a] The stations were grouped as follows: S19 and S9+S7 (background), S3 and S16 (roof), and ALEGA, S12, S11+S10, S20+S13, S14+S15, and S2+S5 (traffic). Sensor pairs are denoted by a plus sign, the lower one is indicated first (see Table 1).

> 0.3, r > 0.5, |FB| < 0.67, and NMSE < 6. As can be seen, the models fulfilled the suggested criteria for all metrics, with the exceptions already highlighted as outliers in the Taylor Diagram. All the models were negatively biased (producing underestimations) and demonstrated some improvement over the reference boundary, except for GRAL at the traffic locations. A closer look at the individual GRAL results for each receptor revealed an exceptional tendency to overpredict at ALEGA monitoring-station, S11 and S20, which are positioned 3–5 m above ground. This could indicate a deficiency in the representation of line sources. PALM delivered the best results for this type of scenario, in terms of FB and NMSE, but completely failed in terms of correlation. Unlike the ATEM and GRAL models, PALM is not driven by observed meteorology data, but by the outputs from the ALADIN model. Therefore, it is not surprising that it may not correctly reproduce the time variability in the measured data. For that reason, capability of the models to reproduce the observed percentiles is explored in Fig. 6 using a Q-Q plot, in which the observed and modeled values are sorted independently for each station and plotted against each other. This reveals that the PALM model outperformed the other two models in reproducing the observed percentiles (slightly overestimating the higher percentiles), while ATEM followed the reference boundary, underestimating the higher percentiles by a factor of 0.5–0.6, and GRAL achieved the opposite, largely overestimating the higher percentiles.

3.2. Spatial variability of concentrations

As shown in Section 3.1, model selection based entirely on summary statistics may be misleading. In this particular situation, one could conclude that the simplest of models, ATEM, is the most suitable for urban applications, as it satisfied all of the acceptance criteria. However, as revealed by the Q-Q plot, the PALM model provided the best results based on the observed percentiles. In this chapter, it is examined what kind of information each model provides regarding the spatial variability in PM_{10} concentrations. As illustrated in the maps of period-averaged concentrations 3 m above ground (Fig. 7), ATEM predicted low concentrations throughout the domain, while GRAL and PALM predicted mostly higher concentrations. In terms of spatial variability, ATEM captured some of the hotspots in the domain, but generally underrepresented the differences between the hotspots and 'cleaner areas'. GRAL and PALM both exhibited high spatial variability, predicting the highest concentrations for those streets with the highest traffic loads. Note that GRAL cannot provide hourly maps in a way that would allow bulk processing for statistical analysis of selected percentiles including boundary conditions. These conjectures are further supported by the fact that the modeled concentrations varied depending on the chosen urban areas, when comparing Legerova and Sokolská streets, all main roads covered by traffic census, minor roads and streets not covered by traffic census, and selected courtyards (Fig. 8). ATEM predicted highly similar pollutant levels in all types of urban areas, whereas the GRAL and PALM predictions exhibited the expected trend in terms of both the median values and scatter. Comparing their median predictions, those of GRAL were higher than those of PALM by about 60 μg m^{-3} for Legerova and Sokolská streets, 41 μg m^{-3} for all main roads, 12 μg m^{-3} for non-counted roads, and 5 μg m^{-3} for courtyards.

In order to fully comprehend the behavior of the model algorithms for built-up areas, it is crucial to evaluate the vertical distribution of concentrations. The vertical concentration profiles in three separate cross-sections throughout the domain are presented (Fig. 9). The first

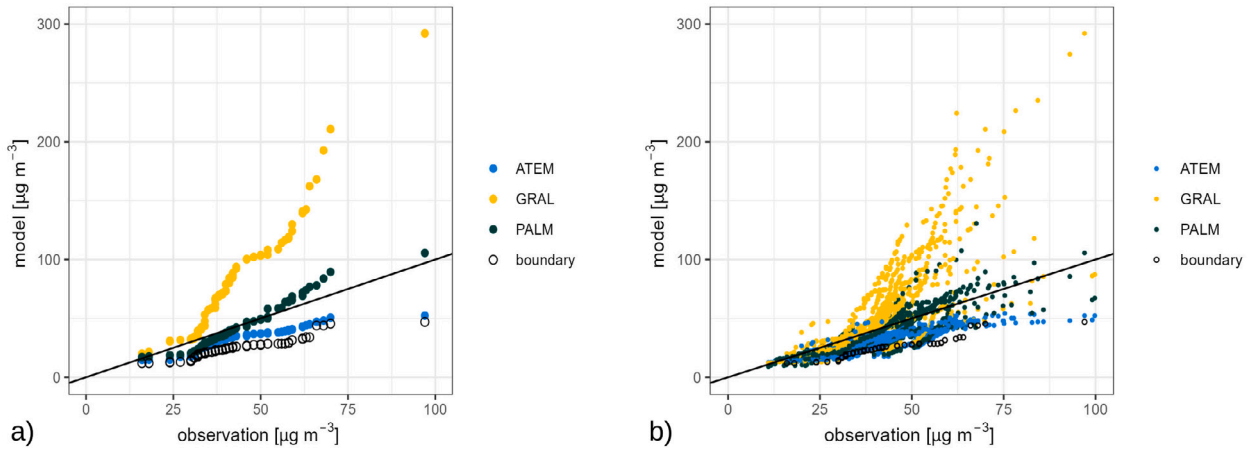

Fig. 6. Q-Q plot based on PM_{10} hourly mean concentrations split by model for ALEGA monitoring-station (a) and for all the stations (b).

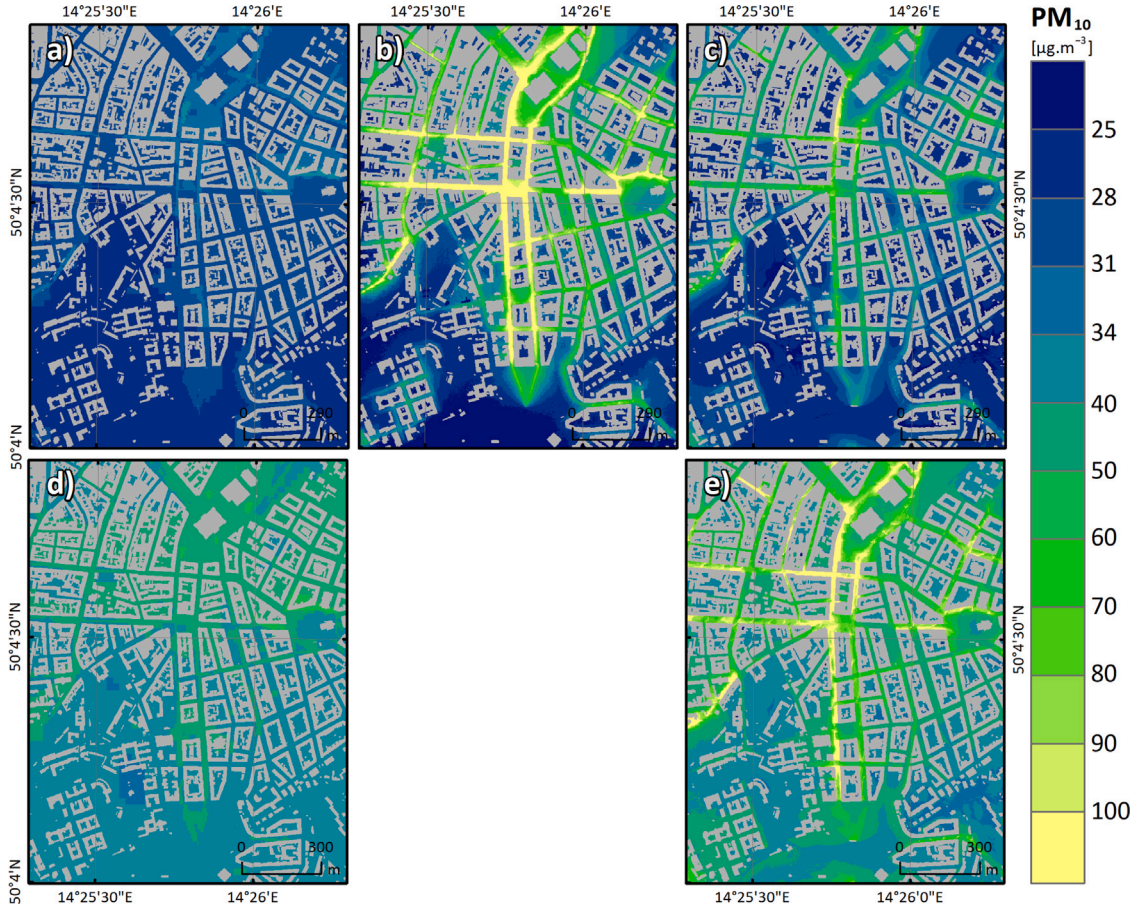

Fig. 7. Mean concentrations (upper row) and 90th percentile of the hourly concentrations (lower row) of total PM_{10} (including boundary concentrations) at 3 m AGL for the period 13–15 February for ATEM (a, d), GRAL (b) and PALM (c, e).

and second vertical profiles (north) represent the effects of buildings in the stagnation of pollutants and the dispersion of traffic emissions on the layers above roofs. The third (south) demonstrates the estimated impact of emissions from the Nusle bridge on the valley below.

Regarding the first two profiles, the most evident differences arise from the lack of a microscale-resolution module in ATEM and the underlying assumption that pollutant concentrations are constant above the plume axis. Consequently, traffic emissions were predicted to spread according to the prevalent wind direction across the streets, with uniform (and generally higher) concentrations in the upper levels.

On the contrary, GRAL and PALM reflected the influence of obstacles on ventilation along the street canyon. Compared to PALM, GRAL predicted greater accumulation of pollution at street ground level, possibly owing to geometrical misrepresentation of road sources.

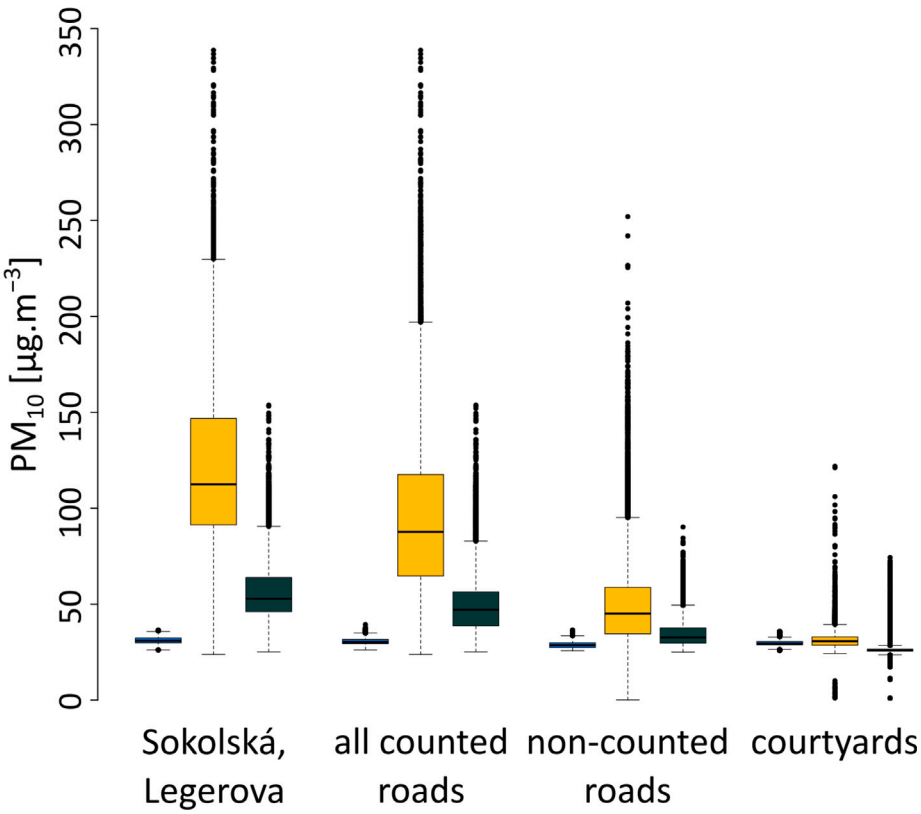

Fig. 8. Variability in the predicted average PM_{10} concentrations in the selected areas (see Fig. A.4) for the period 13–15 February for ATEM (blue), GRAL (yellow) and PALM (dark green) at 3 m AGL. (For interpretation of the references to color in this figure legend, the reader is referred to the web version of this article.)

Moreover, the predicted GRAL concentrations were unrealistically elevated at the facade of buildings. This model behavior, which reflects underdevelopment of the reflection and well-mixed criterion, as well as the stepped resolution of the terrain, has been documented by Oettl et al. [66] as a drawback to GRAL. Additionally, compared to PALM, GRAL predicted a higher influence of upper-level entrainment of PM_{10} into building courtyards. In the case of PALM, pollution stagnation was exhibited in the leeward ground-level corner of Legerova and Sokolská streets, in accordance with the findings of Gidhagen et al. [67], Liu et al. [2], and Park et al. [68] for symmetric street canyons with unity aspect ratio. Based on the cross-sectional results for the Nusle bridge, GRAL estimated the lowest concentrations among the three models, but the patterns of the predictions were similar to those of PALM. Conversely, ATEM predicted an entirely different distribution of concentrations, with a notable increase in concentrations to the east of the bridge, attributed to the overestimated impact of minor roads located in that area of the valley.

4. Discussion

4.1. Limitations and potential sources of error

Many types of error can influence the results of dispersion modeling, the two that appear to be the most important for the present study were identified.

4.1.1. Meteorology and IBC

Microscale models have proven to be sensitive to various factors, including whether dynamic or static input data are used. Microscale simulations are particularly affected by the correct choice of meteorological boundary conditions [69] especially in air-quality modeling for stable weather conditions [10]. To investigate this issue, an additional alternative set of simulations using all three models (ATEM, GRAL and PALM) was provided, using meteorology based on the ICON-D2 [70] model (as a supplementary NWP model). ICON-D2 was chosen as the best model overall from three available mesoscale forecast models (ICON, ALADIN, and WRF) in the evaluation of multiple episodes over the year during the evaluation campaign. However, ICON did not reproduce the wind pattern for the study episode: First, the predicted wind speeds were much lower than those measured above the rooftop at the Karlov station, especially for the first half of the period; and second, for the afternoon of February 13, it did not predict the wind direction well, in fact, it was rotated by ca. 90° (Fig. A.2).

The resulting time-series plots are provided in Fig. 10. While there was almost no change in the predictive behavior of ATEM, that of GRAL and PALM was significantly altered, especially in the first half of the modeled episode in February 2023, for which ICON predicted much lower wind speeds than ALADIN and the values measured at Karlov station. While the GRAL predictions obtained using ICON-D2 were considerably higher, the change in PALM outputs was not as large, except for the pronounced peak for the evening hours on February 13. Resler et al. [10] studied this behavior in detail, concluding that it was a consequence of incorrect predictions of stability by the NWP model.

4.1.2. Resuspension

The levels of dust resuspended from road surfaces exhibit typical seasonal variation, peaking in late winter due to the influence of wintertime maintenance activities of road salting and sanding [71]. Therefore, dust resuspension is probably the most significant source of non-exhaust emissions in this period [72,73], contributing up to 76.7% of the coarse fraction of PM_{10} [74]. For instance, the calculated share of resuspended particles in the total amount of PM_{10} for roads in the modeling domain ranged from 40%–98%, with most of the roads exhibiting a 60%–90% share of resuspended particles (Fig. A.5).

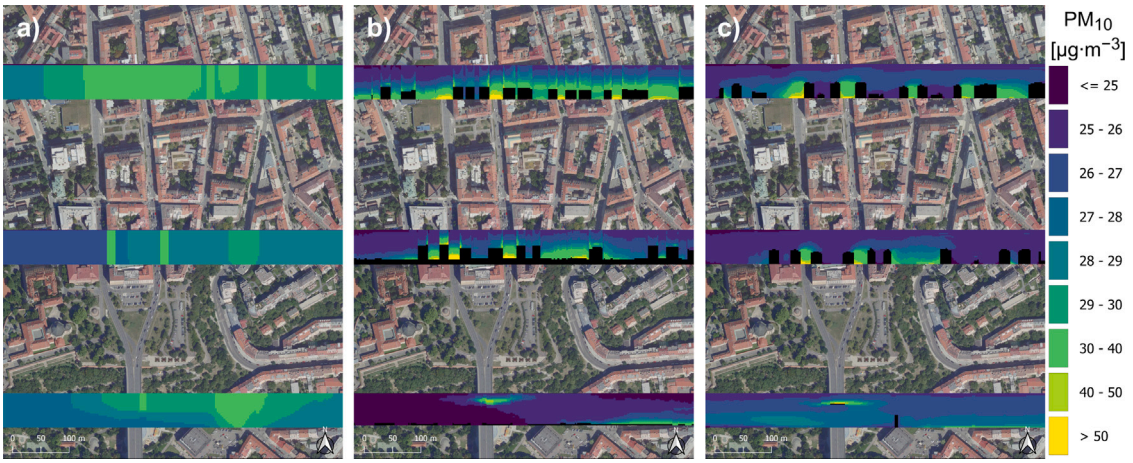

Fig. 9. Vertical cross sections (close-up) of mean concentrations of total PM_{10} (including boundary concentrations) for the period 13–15 February based on ATEM (a), GRAL (b) and PALM (c).

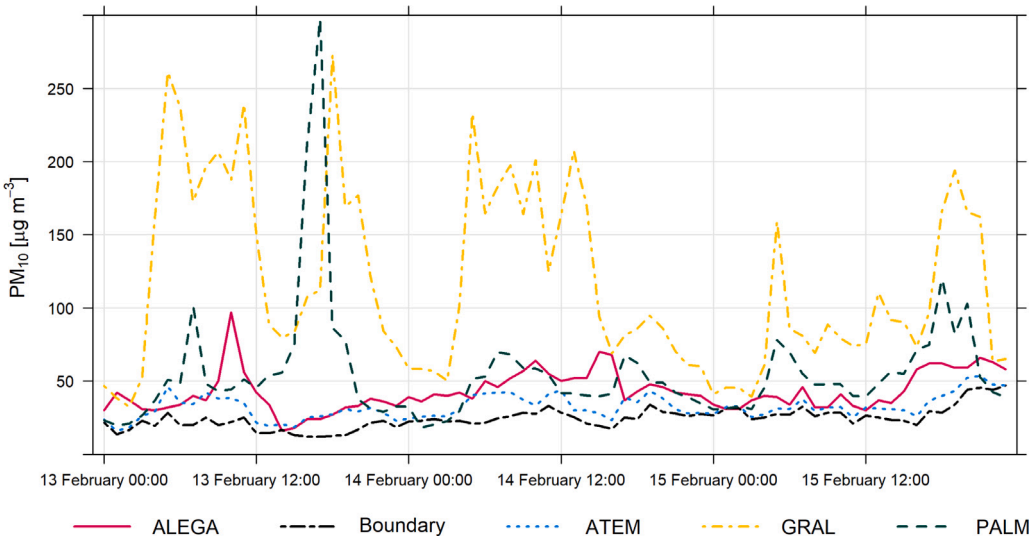

Fig. 10. Time series of PM_{10} concentrations computed by ATEM, GRAL, and PALM with meteorology based on ICON-D2 compared against ALEGA monitoring-station measurements.

Resuspension, which accounts for particles deposited on the road surface that can be dispersed and then redeposited, is influenced by several factors, including traffic volume, the proportion of trucks, vehicle weights and dimensions, driving speed, driving smoothness, the nature of the road surface, the amount of dust particles on the road surface, the road surface material, the state of road surface wear, road cleaning and winter gritting activity, the frequency and intensity of precipitation, wind speed, humidity, and season [55]. Resuspension is calculated using a statistical approach to relate emission rates to the influencing parameters, considering the average fleet composition, vehicle dimensions and weights, and the amount of dust on the road, derived from the average daily vehicle intensity. The amount of dust on the road is considered to decrease as traffic intensity increases. When modeled for short time-steps (such as by hour), these factors may exhibit random bias; therefore, the actual emissions in a particular hour may be several factors greater or less than the average. Similarly, it is not possible to capture data about the random transit of, for example, higher speed vehicles, emergency vehicles, road cleaning (which substantially reduces the amount of dust on the road) or, conversely, the random contamination of the road with more dust. The modeling of resuspension is thus subject to some errors, which are averaged over longer time-intervals. As a consequence, using hourly assessments can lead to significant errors in the modeled resuspension.

To assess the impact of this uncertainty on a particular model, an experiment was performed excluding resuspended particulate matter from the main roads inside the modeling domain (Fig. A.6). The consequent reduction in the predicted concentrations indicates the limit of the uncertainty due to this factor. The adjustment substantially reduced the predicted concentrations at the ALEGA monitoring-station, especially for GRAL. The unrealistic peak observed on February 13 before noon was reduced to a value closer to the observations, improving the modeled trends for the entire episode. The PALM predictions decreased, producing worse results for February 13, but increasing the agreement with observations after noon on February 14, the period of the temperature inversion. In contrast, the ATEM predicted concentrations were closer to the boundary conditions, barely differentiating the impact of emissions. Considering the combined measurements from the ALEGA monitoring-station and LCS (Fig. A.7), the substantial reduction of the transit-related emissions led to the decreased variability of the resulting concentrations, primarily for those that substantially overestimated the observed values. This analysis confirms that potential inaccuracy in resuspended dust estimations can significantly influence the model results, especially for the more sophisticated models.

The sensitivity of the GRAL model to uncertainty in the emissions input data, particularly from non-exhaust emissions, has been reported already [71]. For instance, local formation of secondary aerosols may

increase the uncertainty in predictions, given that it could contribute up to 15% of the emissions during winter. Moreover, a CFD–chemistry coupled model may achieve better agreement with measurement data than conventional simulations that assume particulate-matter emissions to be a passive scalar [75].

4.2. Potential for practical applications

So far, the models have been compared based on the quality of their predictions expressed in terms of correspondence to real conditions. However, additional factors should be considered when judging suitability for practical applications. End-users might be bound by other factors, typically including time and cost constraints, depending on the application. For instance, while an operational forecast might be required by a certain deadline, scenario simulations do not necessarily have tight delivery schedules, but might be constrained by the available budget. Ultimately, the choice of model is not always dictated solely by model performance, but must reflect a compromise between quality, time, and costs. Each of these aspects should be considered as a multifaceted component. When considering time, for instance, it is necessary to consider both the amount of time needed to run the simulations, as well as that required for data-related tasks such as preprocessing, postprocessing, visualization, and interpretation. Cost factors include both the direct costs of computational resources and their operation, and other expenses, such as related to manpower or training.

Choosing the appropriate model thus requires some form of cost–benefit analysis. A SWOT analysis of the three models examined here is presented as an example (Table 3). Notably, this analysis is valid only for the selected models (e.g., some limitations, such as non-suitability for use on high-performance computing (HPC) clusters, or the use of closed-source code, may not be relevant for other Gaussian models). Furthermore, SWOT analyses are subjective, and their results depend substantially on the selected parameters. For instance, considering adherence to open-science standards (as defined, e.g., by UNESCO [76]), while a scientist would likely consider an open-source model to be preferable, a municipality representative not versed in the principles of open-science might not include this parameter in their SWOT analysis.

Computational cost is primarily a measure of the complexity of a simulation in terms of the time and resources required. The computational costs of the model simulations performed here were examined (Table 4). These models differed in computational feasibility by an order of magnitude. While the GRAL model can run on a PC (or even on a powerful 8-core laptop with sufficient memory), ATEM can run on a powerful 8–24-core PC. Here, a 172-core computational node was used to speed up the computation. In contrast, PALM simulations require special HPC multi-node clusters with tens to hundreds of cores and fast inter-node communication. Running an HPC cluster is relatively costly; the most powerful HPCs are usually available only upon request through specialized computational centers, and their use is typically tied to international grants or projects.

These factors impose certain limitations on the appropriateness of each model type for certain applications. PALM, at 1 m resolution, would not be suitable for operational forecasts, owing to the high computation/simulation time ratio required. Longer-term simulations (such as full-year evaluations of air-quality that are periodically performed by meteorological service organizations) are also not feasible using current computing technologies. In fact, simulations can be performed for only a few carefully pre-selected episodes during a year. Typically, these would be situations with unfavorable air quality, such as inversions. Nonetheless, out of the three models compared here, only PALM can perform coupled simulations of meteorology and chemical transport, such as those necessary to evaluate the joint impacts of urban development on biophysical indicators and air quality.

Given its computational requirements, GRAL may provide a good cost–quality balance for detailed assessment of air quality in urban areas. Since GRAL is intended for use primarily by those without particular expertise in CFD modeling, the number of user-provided parameters (such as relaxation factors and logistical aspects related to time-steps) is limited to ensure that the results are numerically stable and represent steady-state conditions. To accommodate this requirement, micro- and mesoscale wind-field models have been simplified in a few respects to guarantee fast and robust simulations for regulatory purposes [77]. Although such simplifying assumptions (such as the binning of meteorological values when calculating wind-fields), have shown to achieve reasonable agreement between observations and predictions in several experiments, even at the city-scale [13,71,78,79], they hinder the possibility to simulate detailed spatio-temporal variation in pollutant concentrations [80]. Moreover, shortcomings have been identified concerning the extent of recirculation zones for idealized wind-tunnel building geometries [77].

Legislation on dispersion models and their requirements presents another important perspective. Models used to assess whether or not air-quality exceeds the thresholds must both generate the corresponding statistics (typically, the annual mean or n-th highest hourly or daily values) and must fulfill data-quality objectives, such as those set by the EU Ambient Air Quality Directive [81]. As it was indicated, even the calculation of annual statistics is complex and can be challenging using the models examined here. ATEM and GRAL face a similar problem, in that they cannot generate annual statistics (especially percentiles) that properly account for boundary conditions (i.e., the contribution of sources outside of the modeling domain). While PALM can achieve this, the computational demands make it feasible to calculate only a limited number of days, from which annual statistics would have to be reconstructed. Standard approaches used in microscale modeling involve the calculation of a set of scenarios for different wind directions and their combination or correction using information on wind speed or measured concentrations (e.g., [33]). However, this approach is not applicable to LES models, as they do not calculate concentrations under steady-state conditions, but rather solve turbulent processes that evolve over time. Therefore, it is necessary to develop and test new methods to estimate annual statistics from a limited number of simulations.

5. Conclusions

The spatio-temporal analysis of the results led to the conclusion that model selection for air quality assessment could be heavily biased by statistical performance metrics, in which the Gaussian model ATEM apparently outperformed the more advanced models. However, based on a detailed examination of the horizontal and vertical patterns of modeled concentrations, ATEM provided limited information on horizontal variability and virtually no information on vertical variability in complex urban environments. Although Gaussian models are commonly used because of their simplicity and conservative results, it was demonstrated that the application at the scale considered in this work could lead to an optimistic idea showing rather low concentrations with respect to reality. In contrast, the development of algorithms incorporating wind-flow fields into the Lagrangian model GRAL and the LES model PALM enabled to reflect and reproduce wind-flow patterns and concentration distributions. Nonetheless, GRAL strongly overestimated concentrations at the street-canyon measurement locations. PALM performed more accurately overall, complying with the statistical quality metrics and generating the most realistic distribution of concentrations.

All three models were sensitive to inaccuracy in their inputs. A sensitivity test using different meteorology data revealed a higher impact on the results for the GRAL and PALM models. For PALM, the substantial underestimation of wind flow by the driving NWP model for a few hours led to a short-term but strong overprediction [10]. The ATEM model was substantially less sensitive to the driving meteorology data. The emissions-reduction test, in which resuspension of PM_{10} on the main roads was excluded, led to a decrease of the variability of the modeled concentrations, primarily for GRAL and PALM. This exclusion reduced the concentrations in street-canyon by up to tens of $\mu g\ m^{-3}$,

Table 3
SWOT analysis of the three models included in the study: ATEM, GRAL, PALM.

	ATEM	GRAL	PALM
Strengths	Low computational costs (can be run on a PC) Relatively low time and labor costs of emissions-data preparation Highly effective for evaluation of selected points in the area of the emission sources Currently used for regulatory purposes in the Czech Republic User-friendly graphical interface	Medium computational costs (can be run on a PC) Open source Includes a user-friendly graphical interface	Captures the full complexity of the urban environment: meteorology and chemistry Open source Active developer community Expanding user community Explicit representation of turbulence in LES mode Extensively validated for different conditions Scales well on HPC
Weaknesses	Only suitable for air quality modeling No chemistry In standard application, includes only average meteorological conditions, in the form of a wind-rose Underestimates average concentrations and their spatial variability Closed-source commercial software that is maintained and operated by a private company Not suitable for HPC	Only suitable for air quality modeling Chemistry included only as a post-processing scheme for NO_X to NO_2 conversion Relatively small community Uses the .NET architecture, which is not widespread in the scientific community and is not suitable for complex atmospheric models	High computational costs (requires HPC cluster) Very-high-resolution input data required Sensitivity to inputs Still under development Requires qualified modeling experts for model setup, running, input collection, and output interpretation Lack of full-scale user-friendly interface
Opportunities	Can easily produce yearly statistics even for non-significant days (from an air-quality point of view) Can be easily improved upon user request depending on the funding availability	In combination with AI that is trained on pre-processed data, such as PALM predictions, it could provide a useful rapid prediction tool	Extensible architecture Options for automation Could be used as a component in an urban 'digital twin' solution Can be used in many urban applications The availability of computational resources is increasing very rapidly and the relative price is declining
Threats	Lack of support/development Diminishing interest in models with limited capabilities	Lack of support/development Lack of understanding and confidence from end-users	Lack of fine-resolution input data Uncertainty in simulation results Lack of understanding and confidence from end-users (not widely used yet in city-planning practice)

Table 4
Computational cost and time demands for each model.

	ATEM[a]	GRAL	PALM-ALAD[b]
Domain (resolution): number of cells	Concentration (24 m): 50 × 66	Mesoscale (50 m): 30 × 38 × 50 Microscale (2 m): 600 × 800 × 40	Parent (10 m): 800 × 800 × 160 Child (2 m): 600 × 800 × 160
Cores used	172	8	Parent: 320 Child: 800
Core-hours	150–200	96	7370 × 128
Real-time for 72 h simulation	2 h	0.5 d (12 h)	34.1 d (818.8 h)
Computation/simulation time ratio	0.03	0.2	10.5

[a] Estimate based on the full-year simulation requiring 17,500 core-hours.
[b] Includes 6 h spin-up time (78 h simulation in total).

most notably for the substantially overestimated predictions. Moreover, it was noted that secondary aerosol formation could potentially affect the estimated mass-concentration and size-distribution of the particulate matter.

Nevertheless, in a real-world application, factors other than model performance need to be considered, from a scientific or even legislative perspective. These include both the available time and financial resources, the availability of high-resolution input data for complex models such as PALM, or the type of application for which the model should be used. For example, the Gaussian model ATEM and the Lagrangian model GRAL can be used to evaluate annual air-quality statistics even in the presence of limitations, whereas in the case of the LES model PALM, further research is required in this respect. Conversely, the more sophisticated models must be used when the application is limited to the detailed evaluation of concentration patterns in street canyons. Moreover, LES models may be the only appropriate choice for the combined evaluation of air quality and other micrometeorological parameters, such as thermal comfort. The future of urban air-quality assessment seems to involve the use of model chains or model ensembles. Together with data-fusion methods, these models can serve as building blocks for the microscale component of integrated urban services. Forthcoming work will be conducted to extend these simulations to address different types of meteorological conditions throughout the year.

Code and data availability

Observations used in this study are available in the repository https://doi.org/10.5281/zenodo.10655033 under the Creative Commons Attribution 4.0 International license. PALM source code and input data used in the simulations are available in the repository https://doi.org/10.5281/zenodo.10998235 under licenses Creative Commons Attribution 4.0 International (data) and GNU General Public License v.3 (source code). The ATEM model is commercially available from https://atem.cz/atem.php. The GRAL model is open-source and is available from https://github.com/GralDispersionModel/. The input data for replication of the ATEM and GRAL simulation can be obtained upon request from the authors.

CRediT authorship contribution statement

William R. Patiño: Writing – original draft, Visualization, Validation, Software, Writing – review & editing. **Ondřej Vlček:** Writing – original draft, Validation, Supervision, Project administration, Methodology, Conceptualization. **Petra Bauerová:** Data curation. **Michal Belda:** Writing – original draft, Validation, Software. **Martin Bureš:** Validation, Software. **Kryštof Eben:** Validation, Software. **Vladimír Fuka:** Validation, Software. **Jan Geletič:** Writing – original draft, Visualization, Validation, Software. **Radek Jareš:** Software. **Jan Karel:** Software. **Josef Keder:** Data curation. **Pavel Krč:** Validation, Software. **Jelena Radović:** Writing – original draft, Validation, Software. **Hynek Řezníček:** Writing – original draft, Validation, Software. **Adriana Šindelářová:** Data curation. **Jaroslav Resler:** Writing – original draft, Validation, Supervision, Software, Project administration, Methodology, Funding acquisition, Conceptualization.

Declaration of competing interest

The authors declare that they have no known competing financial interests or personal relationships that could have appeared to influence the work reported in this paper.

Acknowledgments

The work was financially supported by Norway Grants and the Technology Agency of the Czech Republic (TA ČR) through the KAPPA program (TURBAN project TO01000219) and further by TA ČR through the Environment for Life program (ARAMIS project SS02030031). This publication has been prepared using European Union's Copernicus Land Monitoring Service information; doi: https://doi.org/10.2909/71c95a07-e296-44fc-b22b-415f42acfdf0. PALM simulations, pre- and post-processing were performed on the HPC infrastructure of the Institute of Computer Science of the Czech Academy of Sciences (ICS) supported by the long-term strategic development financing of the ICS (RVO:67985807) and on facilities of the super-computing center IT4I supported by the Ministry of Education, Youth and Sports of the Czech Republic through the e-INFRA CZ (ID:90254). The research was also supported by the Ministry of Education, Youth and Sports of the Czech Republic through the Johannes Amos Comenius program (P JAC) (Natural and anthropogenic georisks project No. CZ.02.01.01/00/22_008/0004605).

Appendix A. Supplementary materials

See Figs. A.1–A.7.

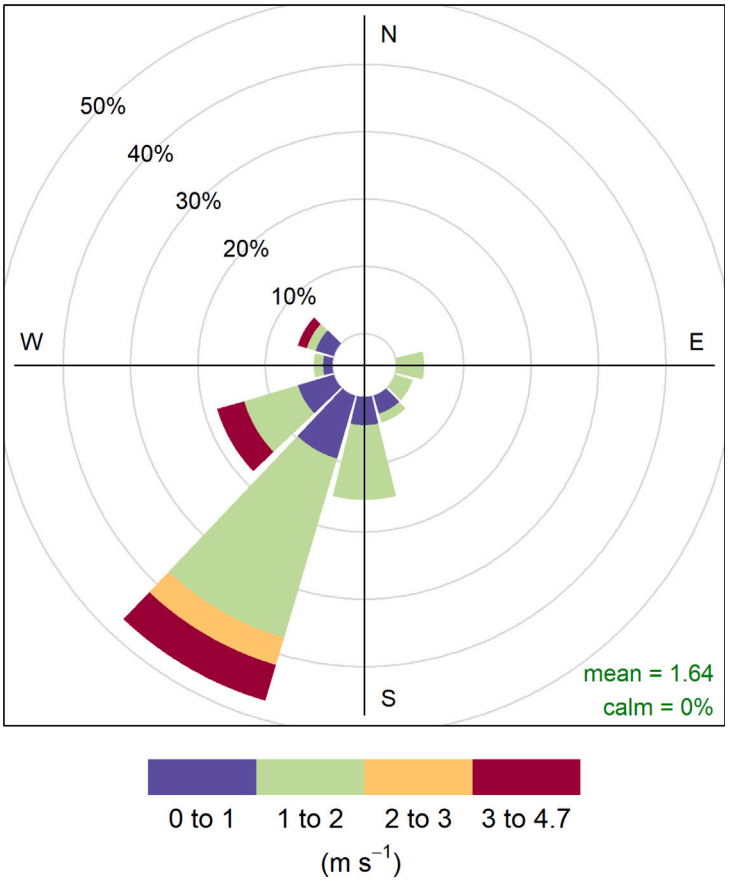

Fig. A.1. Wind-rose of the measured wind vectors at Karlov meteorological station for 13—15 February 2023. The calm-wind limit was set to 0.3 m s^{-1}.

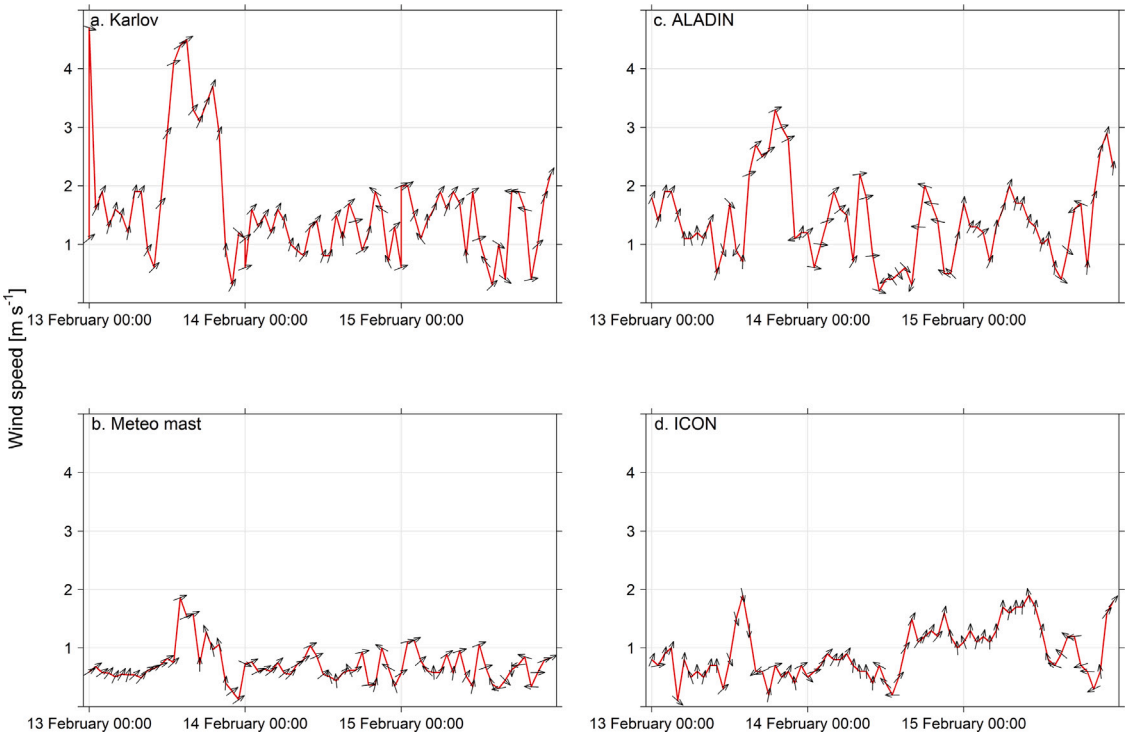

Fig. A.2. Time series of wind speed and direction (arrows) obtained by (a) Karlov meteorological station (30 m AGL), (b) mobile meteorological mast (7.5 m AGL), (c) ALADIN, and (d) ICON.

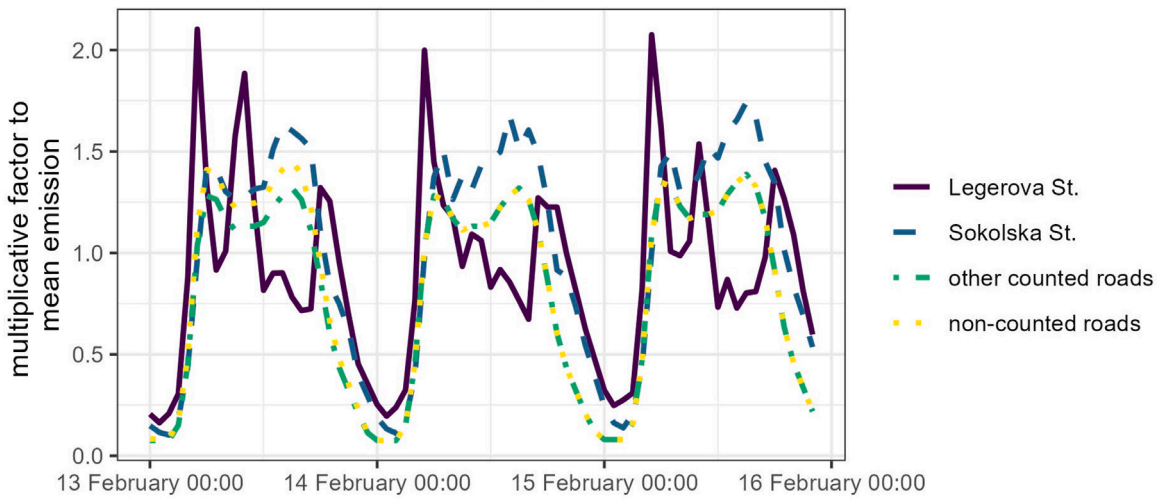

Fig. A.3. Emissions time-profiles for different types of roads. The values displayed correspond to multiplicative factors by which the mean hourly emission needs to be multiplied.

Fig. A.4. Selected areas with a different air quality assumption used for Fig. 8. (a) Sokolská/Legerova, (b) counted roads, (c) non-counted roads, and (d) courtyards.

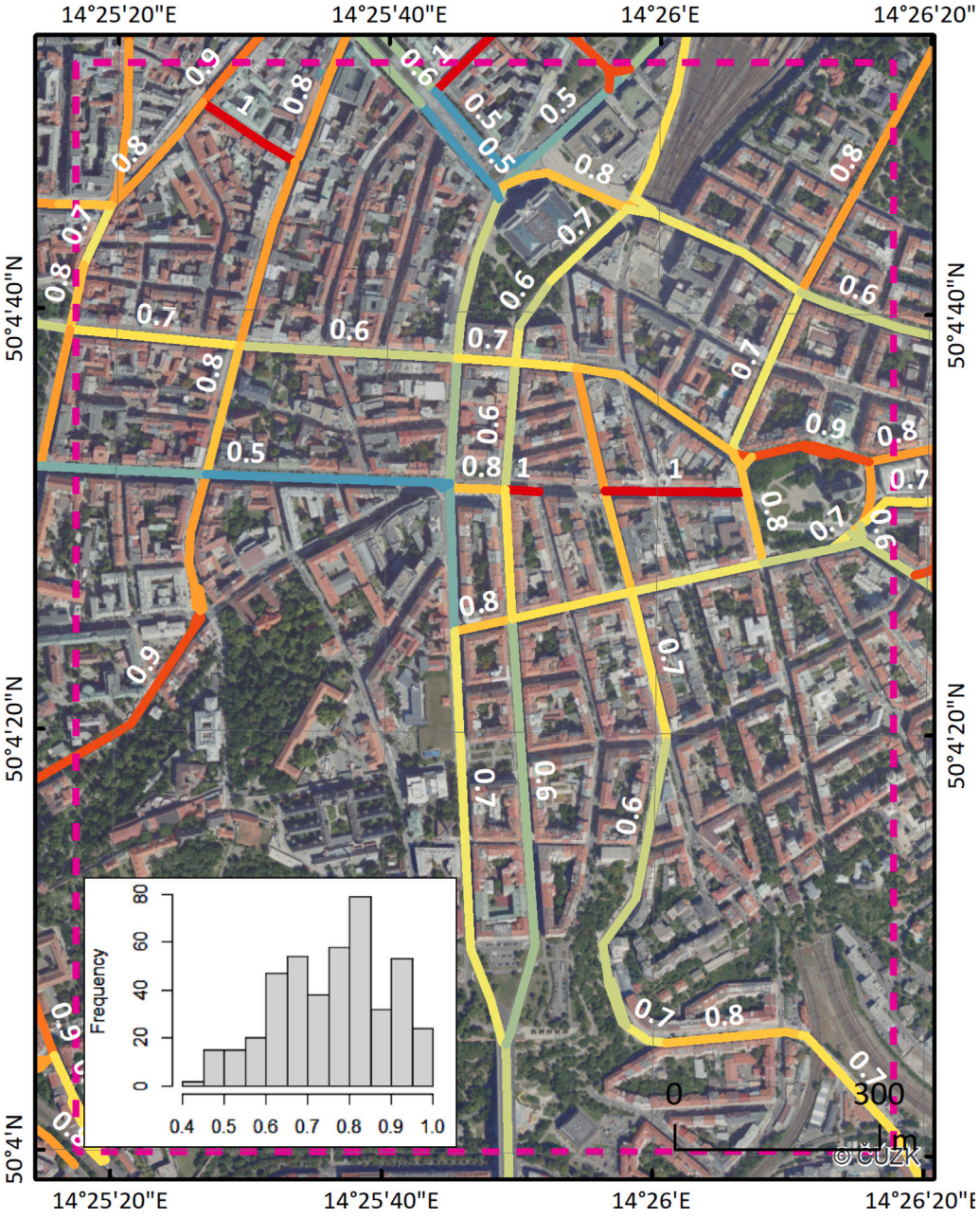

Fig. A.5. Share of resuspended particles in total PM_{10} emissions for the main roads covered by the traffic census. Inset: Frequency distribution of the resuspension ratios for the road segments within the modeling domain.

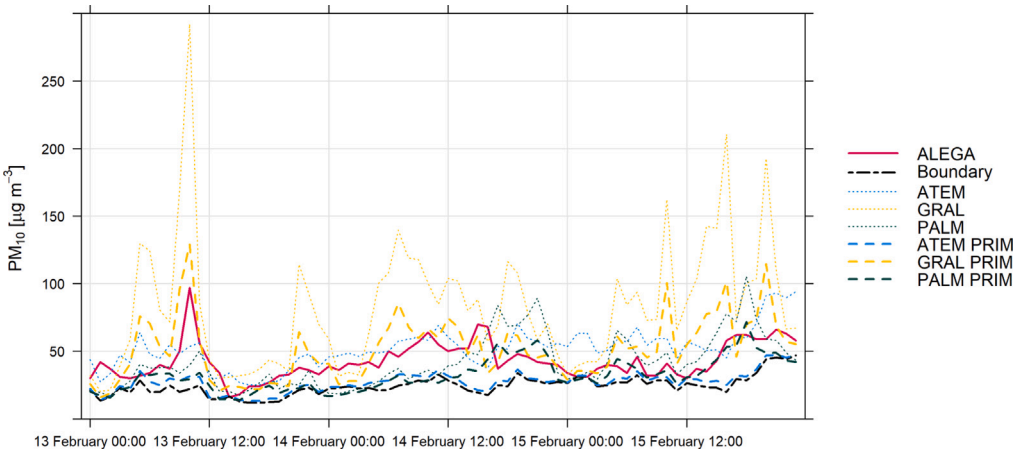

Fig. A.6. Time series of PM_{10} concentrations computed by ATEM, GRAL, and PALM with resuspension, and excluding resuspension from the main roads (PRIM) compared against ALEGA monitoring-station measurement.

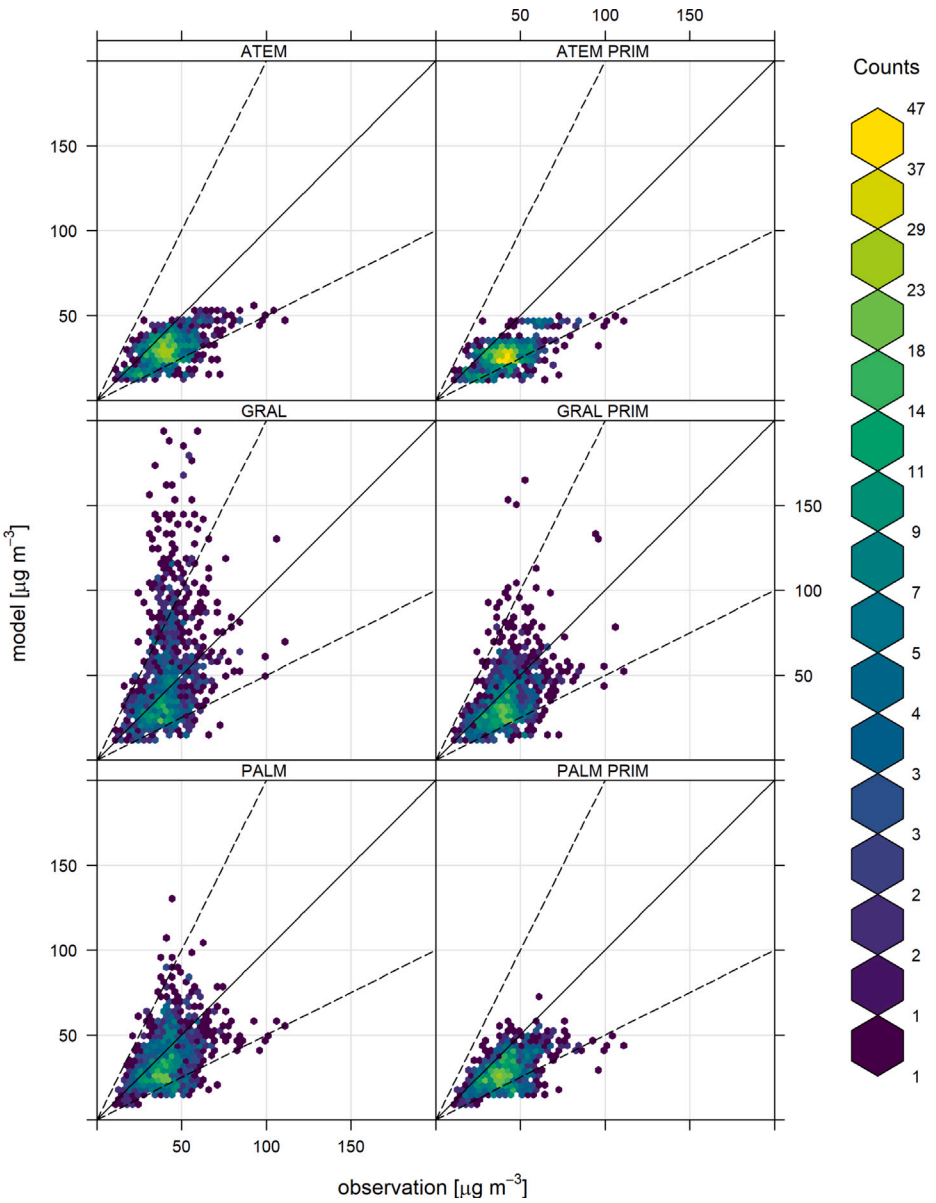

Fig. A.7. Scatter plots of observed concentrations (µg m^{-3}) at ALEGA monitoring-station and LCS against modeled concentrations with resuspension (left) and excluding resuspension from the main roads (right).

References

[1] S. Vardoulakis, B.E. Fisher, K. Pericleous, N. Gonzalez-Flesca, Modelling air quality in street canyons: a review, Atmos. Environ. 37 (2) (2003) 155–182, http://dx.doi.org/10.1016/S1352-2310(02)00857-9.

[2] C.-H. Liu, M.C. Barth, D.Y.C. Leung, Large-eddy simulation of flow and pollutant transport in street canyons of different building-height-to-street-width ratios, J. Appl. Meteorol. 43 (10) (2004) 1410–1424, http://dx.doi.org/10.1175/JAM2143.1.

[3] Y. Dai, A. Mazzeo, J. Zhong, X. Cai, B. Mele, D. Toscano, F. Murena, A.R. MacKenzie, Modelling of deep street canyon air pollution chemistry and transport: A wintertime naples case study, Atmosphere 14 (9) (2023) http://dx.doi.org/10.3390/atmos14091385.

[4] K.W. Lo, K. Ngan, Characterizing ventilation and exposure in street canyons using Lagrangian particles, J. Appl. Meteorol. Climatol. 56 (5) (2017) 1177–1194, http://dx.doi.org/10.1175/JAMC-D-16-0168.1.

[5] P. Brimblecombe, Air Pollution Episodes, World Scientific (Europe), 2017, http://dx.doi.org/10.1142/q0098.

[6] K. Maciejewska, Short-term impact of PM2.5, PM10, and PMc on mortality and morbidity in the agglomeration of Warsaw, Poland, Air Qual. Atmos. Health 13 (6) (2020) 659–672.

[7] WHO, Review of evidence on health aspects of air pollution - REVIHAAP project technical report, 2013, URL https://iris.who.int/handle/10665/341712. [online, cited 30 April 2024].

[8] A. Martilli, B. Sanchez, D. Rasilla, G. Pappaccogli, F. Allende, F. Martin, C. Román-Cascón, C. Yagüe, F. Fernandez, Simulating the meteorology during persistent wintertime thermal inversions over urban areas. The case of Madrid, Atmos. Res. 263 (2021) 105789, http://dx.doi.org/10.1016/j.atmosres.2021.105789.

[9] M. Parra, J. Santiago, F. Martín, A. Martilli, J. Santamaría, A methodology to urban air quality assessment during large time periods of winter using computational fluid dynamic models, Atmos. Environ. 44 (17) (2010) 2089–2097, http://dx.doi.org/10.1016/j.atmosenv.2010.03.009.

[10] J. Resler, P. Bauerová, M. Belda, M. Bureš, K. Eben, V. Fuka, J. Geletič, R. Jareš, J. Karel, J. Keder, P. Krč, W. Patiño, J. Radović, H. Řezníček, M. Sühring, A. Šindelářová, O. Vlček, Challenges of high-fidelity air quality modeling in urban environments - PALM sensitivity study during stable conditions, EGUsphere (2024) 1–35, http://dx.doi.org/10.5194/egusphere-2024-1231.

[11] N. Moussiopoulos, E. Kalognomou, A. Papathanasiou, S. Eleftheriadou, P. Barmpas, C. Vlachokostats, Z. Samaras, G. Mellios, I. Vouitsis, S. Larssen, et al., ETC/ACC street emission ceiling (SEC) exercise, 2005.

[12] M. Moussiopoulos, Z. Samaras, L. Kalognomou, M. Giannouli, S. Eleftheriadou, G. Mellios, Air pollution at street level in European cities, Tech. rep., EEA Tech. Rep, 2006.

[13] D. Oettl, U. Uhrner, Development and evaluation of GRAL-C dispersion model, a hybrid Eulerian–Lagrangian approach capturing NO–NO2–O3 chemistry, Atmos. Environ. 45 (4) (2011) 839–847, http://dx.doi.org/10.1016/j.atmosenv.2010.11.028.

[14] M. Biggart, J. Stocker, R.M. Doherty, O. Wild, M. Hollaway, D. Carruthers, J. Li, Q. Zhang, R. Wu, S. Kotthaus, et al., Street-scale air quality modelling for Beijing during a winter 2016 measurement campaign, Atmos. Chem. Phys. 20 (5) (2020) 2755–2780, http://dx.doi.org/10.5194/acp-20-2755-2020.

[15] A. Martilli, B. Sánchez, J.L. Santiago, D. Rasilla, G. Pappaccogli, F. Allende, F. Martín, C. Roman-Cascón, C. Yagüe, F. Fernández, Simulating the pollutant dispersion during persistent wintertime thermal inversions over urban areas. The case of Madrid, Atmos. Res. 270 (2022) 106058, http://dx.doi.org/10.1016/j.atmosres.2022.106058.

[16] M. Belda, J. Resler, J. Geletič, P. Krč, B. Maronga, M. Sühring, M. Kurppa, F. Kanani-Sühring, V. Fuka, K. Eben, et al., Sensitivity analysis of the PALM model system 6.0 in the urban environment, Geosci. Model Dev. Discuss. 2020 (2020) 1–32, http://dx.doi.org/10.5194/gmd-14-4443-2021.

[17] B. Maronga, S. Banzhaf, C. Burmeister, T. Esch, R. Forkel, D. Fröhlich, V. Fuka, K.F. Gehrke, J. Geletič, S. Giersch, et al., Overview of the PALM model system 6.0, Geosci. Model Dev. 13 (3) (2020) 1335–1372, http://dx.doi.org/10.5194/gmd-13-1335-2020.

[18] A. Kubilay, J. Allegrini, D. Strebel, Y. Zhao, D. Derome, J. Carmeliet, Advancement in urban climate modelling at local scale: Urban heat island mitigation and building cooling demand, Atmosphere 11 (12) (2020) http://dx.doi.org/10.3390/atmos11121313.

[19] T. Godish, J.S. Fu, Air Quality, CRC Press, 2019.

[20] MoE CR, Decree no. 330/2012 coll., on the method of assessing and evaluating the level of pollution, the extent of informing the public about the level of pollution and smog situations, 2012, URL https://www.mzp.cz/www/platnalegislativa.nsf/d79c09c54250df0dc1256e8900296e32/47c2c3c6b17ea2f5c1257a95003c4c03. [in Czech (laws & regulations from Ministry of the Environment); online, cited 30 April 2024].

[21] D. Oettl, M. Kuntner, R. Hofstadler, Documentation of the Lagrangian particle model GRAL (graz Lagrangian model) V23.11, 2023.

[22] D. Anfossi, W. Physick, in: P. Zannetti (Ed.), Lagrangian Particle Models, 2005, pp. 93–161.

[23] A.S. Rood, Performance evaluation of AERMOD, CALPUFF, and legacy air dispersion models using the winter validation tracer study dataset, Atmos. Environ. 89 (2014) 707–720, http://dx.doi.org/10.1016/j.atmosenv.2014.02.054.

[24] E.A. Gilmore, J. Heo, N.Z. Muller, C.W. Tessum, J.D. Hill, J.D. Marshall, P.J. Adams, An inter-comparison of the social costs of air quality from reduced-complexity models, Environ. Res. Lett. 14 (7) (2019) 074016, http://dx.doi.org/10.1088/1748-9326/ab1ab5.

[25] A. Fernandes, S. Rafael, D. Lopes, S. Coelho, C. Borrego, M. Lopes, The air pollution modelling system URBAIR: how to use a Gaussian model to accomplish high spatial and temporal resolutions, Air Qual. Atmos. Health 14 (12) (2021) 1969–1988, http://dx.doi.org/10.1007/s11869-021-01069-9.

[26] N. Holmes, L. Morawska, A review of dispersion modelling and its application to the dispersion of particles: An overview of different dispersion models available, Atmos. Environ. 40 (30) (2006) 5902–5928, http://dx.doi.org/10.1016/j.atmosenv.2006.06.003.

[27] Y. Tominaga, T. Stathopoulos, CFD simulation of near-field pollutant dispersion in the urban environment: A review of current modeling techniques, Atmos. Environ. 79 (2013) 716–730, http://dx.doi.org/10.1016/j.atmosenv.2013.07.028.

[28] Á. Leelőssy, F. Molnár, F. Izsák, Á. Havasi, I. Lagzi, R. Mészáros, Dispersion modeling of air pollutants in the atmosphere: a review, Open Geosci. 6 (3) (2014) 257–278, http://dx.doi.org/10.2478/s13533-012-0188-6.

[29] H. Forehead, N. Huynh, Review of modelling air pollution from traffic at street-level - the state of the science, Environ. Pollut. 241 (2018) 775–786, http://dx.doi.org/10.1016/j.envpol.2018.06.019.

[30] J. Khan, M. Ketzel, K. Kakosimos, M. Sørensen, S.S. Jensen, Road traffic air and noise pollution exposure assessment – A review of tools and techniques, Sci. Total Environ. 634 (2018) 661–676, http://dx.doi.org/10.1016/j.scitotenv.2018.03.374.

[31] J.B. Johnson, An introduction to atmospheric pollutant dispersion modelling, Environ. Sci. Proc. 19 (1) (2022) http://dx.doi.org/10.3390/ecas2022-12826.

[32] M. Pantusheva, R. Mitkov, P.O. Hristov, D. Petrova-Antonova, Air pollution dispersion modelling in urban environment using CFD: A systematic review, Atmosphere 13 (10) (2022) http://dx.doi.org/10.3390/atmos13101640.

[33] F. Martín, S. Janssen, V. Rodrigues, J. Sousa, J. Santiago, E. Rivas, J. Stocker, R. Jackson, F. Russo, M. Villani, et al., Using dispersion models at microscale to assess long-term air pollution in urban hot spots: A FAIRMODE joint intercomparison exercise for a case study in Antwerp, Sci. Total Environ. 925 (2024) 171761, http://dx.doi.org/10.1016/j.scitotenv.2024.171761.

[34] A. Baklanov, C.S.B. Grimmond, D. Carlson, D. Terblanche, X. Tang, V. Bouchet, B. Lee, G. Langendijk, R.K. Kolli, A. Hovsepyan, From urban meteorology, climate and environment research to integrated city services, Urban Clim. 23 (2018) http://dx.doi.org/10.1016/j.uclim.2017.05.004.

[35] P. Bauerová, J. Keder, A. Šindelářová, O. Vlček, W. Patiño, J. Resler, P. Krč, J. Geletič, H. Řezníček, M. Bureš, K. Eben, M. Belda, J. Radović, V. Fuka, R. Jareš, I. Ezau, Measurement report: TURBAN observation campaign combining street-level low-cost air quality sensors and meteorological profile measurements in Prague, EGUsphere (2024) 1–46, http://dx.doi.org/10.5194/egusphere-2024-1222.

[36] B. Czernecki, M. Półrolniczak, L. Kolendowicz, M. Marosz, S. Kendzierski, N. Pilguj, Influence of the atmospheric conditions on PM 10 concentrations in Poznań, Poland, J. Atmos. Chem. 74 (2017) 115–139.

[37] ATEM - Studio of ecological models, J. Karel, R. Jareš, J. Martinovský, R. Polák, E. Smolová, Model ATEM - methodology manual, 2005, URL https://www.atem.cz/soubory/ke_stazeni/IMATEM_metodika.pdf. [In Czech; online, cited 30 April 2024].

[38] J. Bubník, Koldovskỳ, m.: Typizace počasí se zřetelem ke znečištění ovzduší, Böhm B Kol.: Znečištění Ovzduší v Podkrušnohoří. Sbor Prací HMÚ Praha 20 (1974) 101–106.

[39] CHMI, SYMOS'97.Systém modelování stacionárních zdrojů. Metodická příručka, 2014, URL https://www.mzp.cz/C1257458002F0DC7/cz/autorizace/$FILE/OOO-1Metodicka_priruckaSYMOS97-20190708.pdf. (manual) [in Czech; online, cited 30 April 2024].

[40] W.R. Patiño, O. Vlček, V. Volná, Determination of separation distances integrating complaints records analysis and odour dispersion modelling in the czech republic, Sci. Total Environ. 918 (2024) 170812, http://dx.doi.org/10.1016/j.scitotenv.2024.170812.

[41] W.R. Patiño, V.M. Duong, Intercomparison of Gaussian plume dispersion models applied to sulfur dioxide emissions from a stationary source in the suburban area of Prague, Czech Republic, Environ. Model. Assess. 27 (2022) 119–137, http://dx.doi.org/10.1007/s10666-021-09803-4.

[42] D. Oettl, Quality assurance of the prognostic, microscale wind-field model GRAL 14.8 using wind-tunnel data provided by the German VDI guideline 3783-9, J. Wind Eng. Ind. Aerodyn. 142 (2015) 104–110, http://dx.doi.org/10.1016/j.jweia.2015.03.014.

[43] D. Oettl, J. Kukkonen, R.A. Almbauer, P.J. Sturm, M. Pohjola, J. Härkönen, Evaluation of a Gaussian and a Lagrangian model against a roadside data set, with emphasis on low wind speed conditions, Atmos. Environ. 35 (12) (2001) 2123–2132, http://dx.doi.org/10.1016/S1352-2310(00)00492-1.

[44] W.C. Skamarock, J.B. Klemp, J. Dudhia, D.O. Gill, D.M. Barker, M.G. Duda, X.-Y. Huang, W. Wang, J.G. Powers, et al., A description of the advanced research WRF version 3, NCAR Tech Not 475 (2008) 113, http://dx.doi.org/10.5065/D68S4MVH.

[45] NOAA, Ready tools: Pasquill stability classes. PG classes for fluctuations in wind direction and the vertical temperature gradient, 2022, URL https://www.ready.noaa.gov/READYpgclass.php. National Oceanic and Atmospheric Administration.

[46] K.F. Gehrke, M. Sühring, B. Maronga, Modeling of land–surface interactions in the PALM model system 6.0: land surface model description, first evaluation, and sensitivity to model parameters, Geosci. Model Dev. 14 (8) (2021) 5307–5329, http://dx.doi.org/10.5194/gmd-14-5307-2021.

[47] J. Resler, P. Krč, M. Belda, P. Juruš, N. Benešová, J. Lopata, O. Vlček, D. Damašková, K. Eben, P. Derbek, et al., PALM-USM v1. 0: A new urban surface model integrated into the PALM large-eddy simulation model, Geosci. Model Dev. 10 (10) (2017) 3635–3659, http://dx.doi.org/10.5194/gmd-10-3635-2017.

[48] P. Krč, J. Resler, M. Sühring, S. Schubert, M.H. Salim, V. Fuka, Radiative transfer model 3.0 integrated into the PALM model system 6.0, Geosci. Model Dev. 14 (5) (2021) 3095–3120, http://dx.doi.org/10.5194/gmd-14-3095-2021.

[49] A. Hellsten, K. Ketelsen, M. Sühring, M. Auvinen, B. Maronga, C. Knigge, F. Barmpas, G. Tsegas, N. Moussiopoulos, S. Raasch, A nested multi-scale system implemented in the large-eddy simulation model PALM model system 6.0, Geosci. Model Dev. 14 (6) (2021) 3185–3214, http://dx.doi.org/10.5194/gmd-14-3185-2021.

[50] E. Kadasch, M. Sühring, T. Gronemeier, S. Raasch, Mesoscale nesting interface of the PALM model system 6.0, Geosci. Model Dev. 14 (9) (2021) 5435–5465, http://dx.doi.org/10.5194/gmd-14-5435-2021.

[51] B. Khan, S. Banzhaf, E.C. Chan, R. Forkel, F. Kanani-Sühring, K. Ketelsen, M. Kurppa, B. Maronga, M. Mauder, S. Raasch, et al., Development of an atmospheric chemistry model coupled to the PALM model system 6.0: Implementation and first applications, Geosci. Model Dev. 14 (2) (2021) 1171–1193, http://dx.doi.org/10.5194/gmd-14-1171-2021.

[52] P. Termonia, C. Fischer, E. Bazile, F. Bouyssel, R. Brožková, P. Bénard, B. Bochenek, D. Degrauwe, M. Derková, R. El Khatib, et al., The ALADIN system and its canonical model configurations AROME CY41T1 and ALARO CY40T1, Geosci. Model Dev. 11 (1) (2018) 257–281, http://dx.doi.org/10.5194/gmd-11-257-2018.

[53] MEFA, J. Karel, R. Jareš, J. Martinovský, R. Polák, E. Smolová, Transportation emission model, 2013, URL https://www.atem.cz/mefa.php. [in Czech], data upon request.

[54] J. Karel, R. Jareš, J. Martinovský, R. Polák, E. Smolová, Zpráva o dynamické skladbě vozového parku na území hlavní ho města prahy v roce 2020, 2021, URL https://portalzp.praha.eu/jnp/en/environment/for_experts_and_partner_cities/. [in Czech], data upon request.

[55] J. Karel, R. Jareš, J. Martinovský, R. Polák, E. Smolová, K. Šimonová, Metodika pro výpočet emisí částic pocházejících z resuspenze ze silniční dopravy, CENEST, 2015, URL https://www.mzp.cz/C1257458002F0DC7/cz/doprava/$FILE/OOO-resuspenze_metodika-20190708.pdf. [in Czech], data upon request, online [cited 20 April 2024].

[56] EPA, Compilation of air pollutant emission factors, 2011, URL https://www.epa.gov/air-emissions-factors-and-quantification/ap-42-compilation-air-emissions-factors-stationary-sources. AP-42. Section 13.2.1. Paved roads., [online].

[57] J. Karel, R. Jareš, J. Martinovský, R. Polák, E. Smolová, Projekt TH03030496 zmapování a emisní bilance neevidovaných zdrojů emisí znečišťujících látek na území městských aglomerací. Mapa neevidovaných zdrojů emisí znečišťujících látek na území aglomerace CZ01 praha, 2020, URL https://www.atem.cz/neevidovane_zdroje.php. [in Czech], data upon request, Results partly available online [cited 20 April 2024].

[58] EEA, EMEP/EEA Air Pollutant Emission Inventory Guidebook 2019 – Technical Guidance to Prepare National Emission Inventories, European Environment Agency - Publications Office, 2019, http://dx.doi.org/10.2800/293657.

[59] OTE, Gas load profiles - temperature and recalculated TDD, 2024, URL https://www.ote-cr.cz/en/statistics/gas-load-profiles/normalized-lp?set_language=en. [online, cited 20 April 2024].

[60] H.D. Van der Gon, C. Hendriks, J. Kuenen, A. Segers, A. Visschedijk, Description of current temporal emission patterns and sensitivity of predicted AQ for temporal emission patterns, 2011, EU FP7 MACC. URL https://atmosphere.copernicus.eu/sites/default/files/2019-07/MACC_TNO_del_1_3_v2.pdf. TNO Report [cited 17 April 2024].

[61] M. Belda, N. Benešová, J. Resler, P. Huszár, O. Vlček, P. Krč, J. Karlický, P. Juruš, K. Eben, FUME 2.0–flexible universal processor for modeling emissions, EGUsphere 2024 (2024) 1–16, http://dx.doi.org/10.5194/egusphere-2023-2740.

[62] H. Ardeshiri, M. Cassiani, S.Y. Park, A. Stohl, I. Pisso, A.S. Dinger, On the convergence and capability of the large-eddy simulation of concentration fluctuations in passive plumes for a neutral boundary layer at infinite Reynolds number, Bound.-Layer Meteorol. 176 (2020) 291–327, http://dx.doi.org/10.1007/s10546-020-00537-6.

[63] CAMS, Regional production, updated documentation covering all regional operational systems and the ensemble. Following U2 upgrade, february 2020, 2020, URL https://atmosphere.copernicus.eu/sites/default/files/2020-09/CAMS50_2018SC2_D2.0.2-U2_Models_documentation_202003_v2.pdf. CAMS Report [online, cited 21 April 2024]. METEO-FRANCE.

[64] J.C. Chang, S.R. Hanna, Air quality model performance evaluation, Meteorol. Atmos. Phys. 87 (1) (2004) 167–196, http://dx.doi.org/10.1007/s00703-003-0070-7.

[65] S. Hanna, J. Chang, Acceptance criteria for urban dispersion model evaluation, Meteorol. Atmos. Phys. 116 (3) (2012) 133–146, http://dx.doi.org/10.1007/s00703-011-0177-1.

[66] D. Oettl, M. Kuntner, F. Manansala, Recommendations when using the GRAL/GRAMM modelling system V21.09, 2020, URL https://github.com/GralDispersionModel/GRALRecommendations.

[67] L. Gidhagen, C. Johansson, J. Langner, G. Olivares, Simulation of NOx and ultrafine particles in a street canyon in Stockholm, Sweden, Atmos. Environ. 38 (14) (2004) 2029–2044, http://dx.doi.org/10.1016/j.atmosenv.2004.02.014.

[68] S.-J. Park, J.-J. Kim, M.J. Kim, R.J. Park, H.-B. Cheong, Characteristics of flow and reactive pollutant dispersion in urban street canyons, Atmos. Environ. 108 (2015) 20–31, http://dx.doi.org/10.1016/j.atmosenv.2015.02.065.

[69] J. Radović, M. Belda, J. Resler, K. Eben, M. Bureš, J. Geletič, P. Krč, H. Řezníček, V. Fuka, Challenges of constructing and selecting the "perfect" boundary conditions for the large-eddy simulation model PALM, Geosci. Model Dev. 17 (7) (2024) 2901–2927, http://dx.doi.org/10.5194/gmd-17-2901-2024.

[70] D. Reinert, F. Prill, H. Frank, M. Denhard, M. Baldauf, C. Schraff, C. Gebhardt, C. Marsigli, G. Zängl, DWD database reference for the global and regional ICON and ICON-EPS forecasting system, 2020, DWD 2023Available online. URL https://www.dwd.de/DWD/forschung/nwv/fepub/icon_database_main.pdf. [cited 20 April 2024].

[71] D. Oettl, Modelling of primary PM10 concentrations for the city of Graz, Austria, Hrvatski Meteorol Časopis 43 (43/1) (2008) 375–379.

[72] P. Pant, R.M. Harrison, Estimation of the contribution of road traffic emissions to particulate matter concentrations from field measurements: A review, Atmos. Environ. 77 (2013) 78–97, http://dx.doi.org/10.1016/j.atmosenv.2013.04.028.

[73] M. Penkała, P. Ogrodnik, W. Rogula-Kozłowska, Particulate matter from the road surface abrasion as a problem of non-exhaust emission control, Environments 5 (1) (2018) http://dx.doi.org/10.3390/environments5010009.

[74] D. Jandacka, D. Durcanska, Seasonal variation, chemical composition, and PMF-derived sources identification of traffic-related PM1, PM2.5, and PM2.5–10 in the air Quality Management Region of Žilina, Slovakia, Int. J. Environ. Res. Public Health 18 (19) (2021) http://dx.doi.org/10.3390/ijerph181910191.

[75] C. Lin, Y. Wang, R. Ooka, C. Flageul, Y. Kim, H. Kikumoto, Z. Wang, K. Sartelet, Modeling of street-scale pollutant dispersion by coupled simulation of chemical reaction, aerosol dynamics, and CFD, Atmos. Chem. Phys. 23 (2) (2023) 1421–1436, http://dx.doi.org/10.5194/acp-23-1421-2023.

[76] UNESCO, Recommendation on open science OPENSCIENCE, 2021, URL https://unesdoc.unesco.org/ark:/48223/pf0000379949. [online, cited 30 April 2024].

[77] D. Oettl, Evaluation of the revised Lagrangian particle model GRAL against wind-tunnel and field observations in the presence of obstacles, Bound.-Layer Meteorol. 155 (2) (2015) 271–287.

[78] A. Berchet, K. Zink, C. Muller, D. Oettl, J. Brunner, L. Emmenegger, D. Brunner, A cost-effective method for simulating city-wide air flow and pollutant dispersion at building resolving scale, Atmos. Environ. 158 (2017) 181–196, http://dx.doi.org/10.1016/j.atmosenv.2017.03.030.

[79] A. Berchet, K. Zink, D. Oettl, J. Brunner, L. Emmenegger, D. Brunner, Evaluation of high-resolution GRAMM–GRAL (v15.12/v14.8) NO_x simulations over the city of Zürich, Switzerland, Geosci. Model Dev. 10 (9) (2017) 3441–3459, http://dx.doi.org/10.5194/gmd-10-3441-2017.

[80] D. Oettl, A multiscale modelling methodology applicable for regulatory purposes taking into account effects of complex terrain and buildings on pollutant dispersion: a case study for an inner Alpine basin, Environ. Sci. Pollut. Res. 22 (22) (2015) 17860–17875.

[81] European Union, Directive 2008/50/EC of the European parliament and of the council of 21 may 2008 on ambient air quality and cleaner air for Europe, 2008, URL https://eur-lex.europa.eu/eli/dir/2008/50/2015-09-18.